Akademie věd České republiky

Teze disertace
k získání vědeckého titulu "doktor věd"
ve skupině věd **Chemické vědy**

Heterogenní reakce oxidu uhličitého s kyslíkatými minerály

Komise pro obhajoby doktorských disertací v oboru

Analytická chemie

Svatopluk Civiš

Ústav fyzikální chemie J. Heyrovského v Praze

Praha, listopad 2017

Obsah

Résumé

Molecular spectroscopy is constantly and dynapmically developing technique in its fundamental aspects and applications. This technique continues in its fascinating possibilities of deeper understanding of the basic building blocks of matter and their interaction with electromagnetic radiation. It generates new possibilities for practical applications in industry, chemistry, astronomy, geology, biology, medicine, information technology and many other disciplines.

Massive development records all spectroscopic experimental techniques. Over the past twenty years, old types of classical grating spectrometers have been replaced by Fourier Transform spectrometers. However, these are already extruded by sensitive laser techniques, enabling sub-Doppler observation. The long multiple cuvettes have disappeared from the basements of the institutions and were replaced by hundred kilometers optical path cells inside of the laser resonator. These devices are no longer linked on Earth-based laboratory applications only, but they are used on board of robotic rovers Spirit, Opportunity, and Curiosity on Mars. The Mars Science Laboratory and its rover centerpiece, Curiosity, is the most ambitious Mars mission yet flown by NASA.

Similarly to technology, a huge development process has also taken place in theoretical scientific approaches. More and larger molecules, their interactions and dynamics are being studied. The development of computer technology is constantly shifting their boundaries and possibilities.

A whole new field of nanotechnology applications such as the study of molecules and ion clusters and their interactions, satellite Earth detections, astrophysical applications in all spectral areas, exploration of the expansion of the Universe using state-of-the-art cosmic technologies outside our planet, the study of chemical dynamics using ultra-fast and ultra-power lasers, femtochemistry, laser cooling and the study of individual atoms or ions in ion traps, remote lidar sensing in the environment and, last but not least, computer tomography, including three-dimensional magnetic

resonance of the brain in medicine.

From all this, which has not been listed, it is clear how immense dynamic development of the spectroscopic and nanotechnology disciplines is experienced. It is very difficult to estimate their current theoretical and experimental limits, making it difficult to predict the direction of their development.

In this doctoral thesis I present part of my professional activity focused on the combination of material chemistry of semiconductor nanostructured systems with spectroscopic highly resolved techniques. This paper summarizes the research focused on the description of behavior of semiconductor systems of titanium oxide materials and their interaction with carbon dioxide. In connection with a number of publications describing the thermal interaction of oxygen atoms with the TiO_2 surface (the first part of this work), other very interesting properties have been discovered that fall within the field of photochemistry. By studying these features, the scope of application of crystalline and non-crystalline semiconductor materials has expanded across a range of technologies aimed at photochemical conversion of carbon dioxide to methane. A process called "methanogenesis" has even helped to explain some processes that work in the same way as in the laboratory on the planets of our solar system or even beyond it.

Prague, November 2017
               Svatopluk Civiš

1.   Spontaneous Oxygen Isotope Exchange between Carbon Dioxide and TiO₂

1.1 Introduction

Nanostructured TiO_2 has attracted considerable interest due to its numerous applications in photocatalysis, solar cells, gas sensors, Li-ion batteries, electrochromics and catalysis[1, 2]. These applications require a detailed understanding of the surface science of solid titania (for review for example see Ref. [3]). Chemical processes on the titania surface, both thermally and photochemically

activated, can be conveniently followed by oxygen isotope labeling. These reactions have been carefully studied since the middle of the last century(4–12). The traditional approach is based on the use of 'ordinary' $Ti^{16}O_2$ exposed to gaseous reactants which comprise various ^{18}O-isotope labeled molecules, like $H_2^{18}O$ or $^{18}O_2$ with their corresponding ^{16}O-isotope counterparts. The isotope exchange (e.g. between $^{18}O_2$ (g) and $^{16}O_2$ (g)) may or may not involve the replacing of the lattice oxygen (^{16}O) in titania by ^{18}O. In particular, the reactions of $H_2^{18}O$ on photoexcited titania allowed the addressing of fundamental questions relevant to photocatalysis(13–15), and this approach is smoothly extendable to photoassisted isotopic exchange reactions involving other molecules such as gaseous oxygen(11), formic acid(16, 17), alcohols(18), carbon monoxide and carbon dioxide(10, 17, 19, 20) or carbonates(17).

A variant of the strategy of employing 'ordinary' $Ti^{16}O_2$ for the isotope exchange is the use of titania with a deliberately ^{18}O-enriched surface. This material can be prepared by simply exposing $Ti^{16}O_2$ to $^{18}O_2$ at 750 K(21) or to $H_2^{18}O$ with simultaneous UV irradiation(18) or by electrochemical oxidation in an ^{18}O-containing electrolyte solution(16). In all cases, the isotope exchange $Ti^{16}O_2/Ti^{18}O_2$ is restricted to the surface layers only, and is hardly perfect in these products. For instance, the thermal reaction with oxygen gas provided an ^{18}O-enriched surface of titania with an $^{18}O/^{16}O$ ratio of 2.5(21). Reports on the isotopically pure solid $Ti^{18}O_2$ are surprisingly scarce in the literature. To the best of our knowledge, there is only one paper dealing with the transformation of titanium nitride TiN to TiO_2 in oxygen ($^{18}O_2$) plasma(22). Although this reaction could, in principle, lead to a pure solid $Ti^{18}O_2$, the product was not characterized in Ref. (22). Hence, one of the initial motivations for this study was to synthesize pure $Ti^{18}O_2$ in a defined way. It is obvious that this material would allow the reconsideration of the classical works on the isotopic exchange of ^{18}O on the gas/solid(12) oxide interface. In particular, the release of lattice oxygen and its transfer to the surrounding molecules can be studied on a clean system, in which solely the solid oxide is isotopically labeled. The investigation of adsorption, and catalytic and photocatalytic processes in the 'reverse direction', that is from ^{18}O-labeled oxide towards gaseous molecules at the interface could, obviously, bring novel inputs to this old(4–12) but evergreen(11, 13–15, 18) story.

We have explored the oxygen isotope $^{16}O/^{18}O$ exchange between gaseous $C^{16}O_2$ and solid $Ti^{18}O_2$. Although there have been several earlier works aimed at isotope exchange reactions involving carbon dioxide, the reactions have been typically studied either on the $C^{18}O_2/Ti^{16}O_2$ system(19) or on a complicated gaseous mixture containing, besides $C^{16}O_2$, also $^{18}O_2$ or $H_2^{18}O$ and ordinary $Ti^{16}O_2$(10, 17) Carbon dioxide offers several advantages as the target molecules for these studies: (i) The isotope exchange can be readily followed by high-resolution FTIR; (ii) It is the final product of the photocatalytic oxidation of organic molecules; (iii) the adsorption mechanism of CO_2 is known in detail and moreover, it is of prospective environmental impact for CO_2 removal from the atmosphere (for review of isotope effects in atmospheric CO_2 and other gases see Ref.(23). The present measurement in dark mixtures has, as its primary goal, the determination of the time-scale of the spontaneous isotope exchange between carbon dioxide and solid TiO2. Besides simply affirming that the spontaneous reaction cannot compete with the induced rapid processes in the laser-exposed or UV lamp-illuminated cases, we quantify the spontaneous process by evaluating its absorption vibrational spectra, and we sketch the corresponding reaction mechanism.

1.2 Synthesis of materials

The synthesis of $Ti^{18}O_2$ was carried out in a closed all-glass vacuum apparatus. Titanium tetrachloride was twice distilled in the vacuum before use. 1g of $H_2^{18}O$ (^{18}O 97 %) was frozen out in high vacuum by liquid nitrogen, and the ice was contacted with 2.8 ml of $TiCl_4$ vapor through a glass-breakable valve. After the mixing of both reactants, the cooling bath was removed and the reaction mixture was released at room temperature overnight. The produced HCl was collected in a side ampoule cooled by liquid nitrogen. Subsequently, the solid product was heated at 200ºC overnight in the still-closed vacuum apparatus, while the HCl trap remained in the liquid nitrogen cooling bath. The HCl-trap was then sealed off. Finally, the apparatus was opened in a glove box under Ar and the solid white powder was collected. This product is subsequently abbreviated as T200. The material was stored under Ar at room temperature. In the next synthetic step, part of the T200 powder was

heated at 450ºC in a vacuum (10^{-5} Pa) for 30 hours. This material is subsequently abbreviated as T450. Both samples were characterized by X-ray diffraction (Bruker D8 Advance diffractometer; CuKα radiation), which exhibited the pattern of pure anatase, data not shown. BET from surface areas were calculated from N_2 adsorption isotherms (Micromeritics ASAP 2020 instrument). The samples were degassed at 400ºC in the vacuum prior to measurement. The BET surface area was found to be 31 m^2/g independent of the synthetic history (T200/T450).

1. Light–induced isotopic exchange between CO_2 and $Ti^{18}O_2$ Photoassisted isotope exchange was studied using $Ti^{18}O_2$ calcined in a vacuum at 200 ºC only (sample T200). The 20 cm long optical cell was filled on a vacuum line with 0.8 g of T200 powder and subsequently with 2 Torr of $C^{16}O_2$. The obtained spectrum in the region of 2000-4000 cm^{-1} is shown in Figure 1 (curve b) together with the reference spectrum of carbon dioxide in titania-free optical cell (Fig. 1, curve a). A rotation-vibration band of HCl was detected in the 2800-3000 cm^{-1} spectral region, and small amount of water (mostly $H_2^{16}O$) is apparent by the band at 3600-3800 cm^{-1} (Fig. 1 curve b). Hydrogen chloride is obviously an impurity in the T200 sample: HCl is a product of the synthesis of T200 (reaction of $TiCl_4$ with $H_2^{18}O$), and by calcination at 200ºC in a closed apparatus it is not quantitatively removed. The adsorbed HCl is, released from T200 into the gas phase of our optical cell. Desorption of HCl from T200 occurs already in dark (Fig. 1b) and progresses upon illumination with UV laser (Fig. 1c-d).

However, upon UV-photoexcitation, we observe additional processes beyond the HCl desorption. In the actual experiment, the surface of T200 was irradiated with 4500 pulses of the XeCl laser (308 nm, energy of 180 mJ) which were focused by a quartz lens straight onto the T200 surface through the calcium fluoride window of the optical cell. After the irradiation of the T200 surface with the laser, additional rotation-vibration bands of methane and acetylene were identified in the gaseous phase while the concentration of $H_2^{16}O$ increased (Fig. 1, curve c). Direct photocatalytic conversion of CO_2 into CH_4 a C_2H_2 occurred on the surface of illuminated $Ti^{18}O_2$. Part of the unfocused laser radiation passed through the gaseous CO_2, which was partially broken down into CO. This molecule is identified by a rotation-vibration band in the region of 2050-2200

cm^{-1} (Fig. 1c-d). The sample was stored at temperature of 30 °C and the spectra were measured after 50 and 75 hours without UV-laser irradiation. A rotation-vibration band of water (3600-3800 cm^{-1}) increased in intensity. The occurrence of $H_2^{16}O$ in the gaseous phase over the CO_2/T200 interface, both in dark and upon illumination deserves a special attention. All the main absorption rotation-vibration lines belonged to $H_2^{16}O$, (the lines of $H_2^{18}O$ appeared only in their natural isotopic abundance). Concerning the water molecules which are released or created, no exchange of oxygen atoms ^{18}O from the solid phase ($Ti^{18}O_2$) took place.
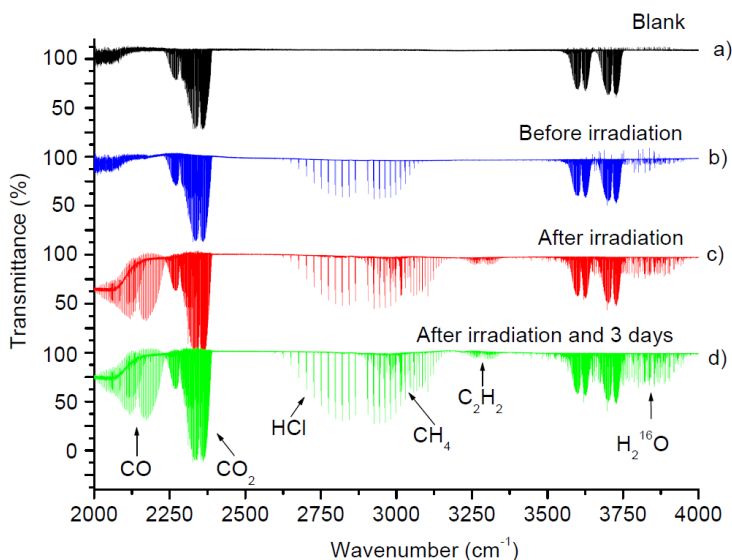

Fig.1: Comparison of the a) $C^{16}O_2$ spectrum with b) the spectrum of the gas phase in the mixture of $Ti^{18}O_2$ (sample T200) and $C^{16}O_2$, c) ditto after the irradiation with 4500 pulses of the XeCl laser, 308 nm, pulse width 28 ns, energy 180 mJ and spectrum d) ditto after 75 hours in dark at 30°C.

The comparison of the reference spectra of methane and acetylene with the spectrum measured after the UV- laser irradiation

of the $Ti^{18}O_2$ (T200) surface in a cell with $C^{16}O_2$ (b), is given in Figure 2.
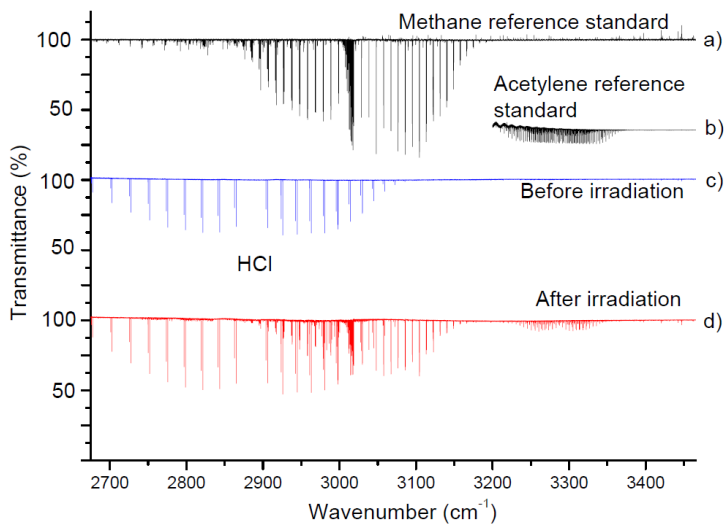

Fig. 2: The reference spectra of a) methane and b) acetylene compared with the c) sample without irradiation and d) the sample after irradiation with 4500 pulses from the XeCl laser, 308 nm, pulse width 28 ns, energy 180 mJ.

Carbon monoxide was created by laser irradiation in the cell (breakdown of CO_2); part of the spectrum is in Figure 3. A small amount of $C^{16}O$ was generated from the gaseous CO_2. $C^{18}O$ was not generated in the cell and the amount of $C^{16}O$ remained constant after 75 hours.
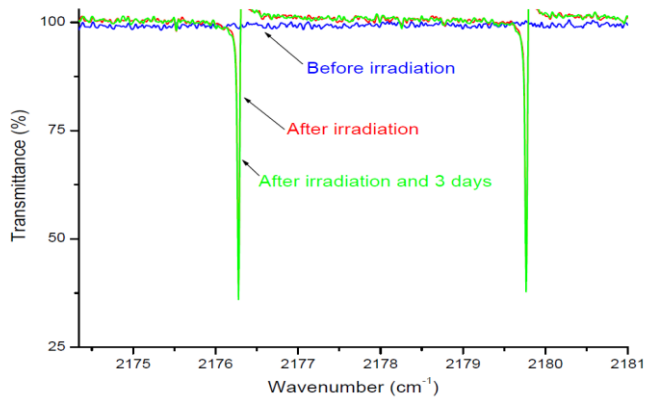
Fig. 3: $C^{16}O$ rotation-vibration lines in the spectrum before the $Ti^{18}O_2$ (T200) irradiation (blue), after the irradiation with 4500 pulses from the XeCl laser (red) and after 75 hours (green).
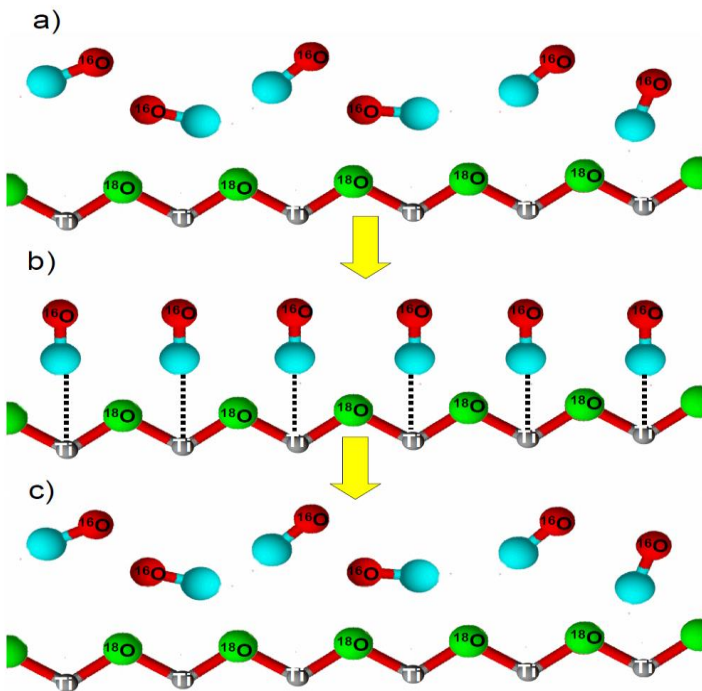
Fig. 4: Diagram of the isotope exchange between the surface of crystallic $Ti^{18}O_2$ and carbon monoxide. CO binds straight to the titanium atom. After the laser irradiation or thermally at low pressure, this complex breaks back into $C^{16}O$.

CO adsorption on anatase and rutile TiO_2 has been studied previously[24]. The observed infrared bands (2192 and 2209 cm^{-1}) were assigned to adsorbed CO bonded to Ti^{4+} ions with a binding energy of 17 kcal/mol[25]. This direct binding of CO to the metal atom (see Fig. 4) explains the fact that the isotope exchange does not take place between the oxygen in the carbon monoxide molecule and the oxygen in the structure of $Ti^{18}O_2$.

In the case of the reaction of CO_2 with $Ti^{18}O_2$ (Sample T200), the spectral intensity of individual rotation-vibration lines of CO_2 could be observed in the v_3 region of the spectral band where the

spectra of all three isotopologues (^{16}O-C-^{16}O, ^{18}O-C-^{16}O, ^{18}O-C-^{18}O) overlap(26). Figure 5 shows the reference spectrum of ^{16}O-C-^{16}O (black) together with the rotation-vibration transitions of individual isotopologues of carbon dioxide from the measured spectra. In the non-irradiated mixture of T200 and C^{16}O$_2$ no additional lines corresponding to the individual rotation-vibration transitions of ^{18}O-C-^{16}O and ^{18}O-C-^{18}O molecules were found (Fig. 5, blue curve) and the resulting spectrum fully corresponds to the spectrum of the pure C^{16}O$_2$.

Only after the irradiation of the sample with 4500 pulses by the UV laser the ^{18}O-C-^{16}O and ^{18}O-C-^{18}O molecules appear in the gaseous phase (Fig. 5, red curve). Their concentration grew with time (Fig. 5, green curve). The individual lines in the spectra have been fitted and quantified. Thus calculated concentrations of individual isotopologues (Figure 6) showed an incremental jump (after the laser irradiation) and a moderate increase (instead of decrease which one would intuitively expect) of the ^{16}O-C-^{16}O isotopologue. The isotopologue ^{18}O-C-^{18}O remained constant after the irradiation and the isotopologue ^{18}O-C-^{16}O showed a slight increase over time in the mixture. The results shown in Figures 5.

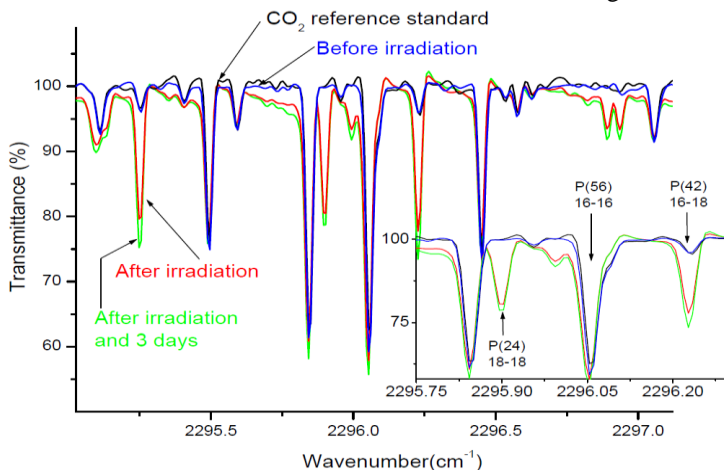Fig.5: Several rotation-vibration lines of the ν_3 band of C^{16}O$_2$ in the spectral range 2295-2298 cm^{-1} (reference spectrum - black) together with the spectra of carbon dioxide (2 Torr) measured immediately

after irradiation by the XeCl laser (red), and after 75 hours (green). The absorption cell contained 0.8g of $Ti^{18}O_2$ in the powder form (T200) spread over the walls of the glass reaction cell.

1.3 Mechanism of the light induced oxygen exchange between $Ti^{18}O_2$ and $C^{16}O_2$

TiO_2 heated to a temperature of 200°C (sample T200) showed low oxygen exchange activity. The process of isotope exchange and the adsorption of CO_2 are to a large extent influenced by the presence of water and OH groups on the surface of the TiO_2(27). After the irradiation of the sample, the ^{16}O-C-^{18}O and ^{18}O-C-^{18}O concentrations in the gaseous phase increased by a jump and then a slow process of spontaneous isotope exchange took place in the dark. A very interesting phenomenon is the release of adsorbed CO_2, which is almost completely composed of $C^{16}O_2$ and the parallel process of the release of water from the surface of the sample, which is composed of $H_2^{16}O$ (see Fig.1). The release of water can be explained on the basis of the breakdown of the carbonic acid bonded to the surface of TiO_2:

$$H_2CO_3 \rightarrow CO_2 + H_2O$$
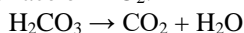
As at the beginning of the experiment, $H_2^{18}O$ is adsorbed on the surface of $Ti^{18}O_2$, and the carbonic acid is composed of a mixture of ^{16}O and ^{18}O.

The increased concentration of $H_2^{16}O$ in the gaseous phase above the TiO_2 surface after 75 hours can be explained on the basis of the breakdown of the carbonate complex and the spontaneous isotope exchange reaction taking place in the dark:

$$H_2^{18}O + {}^{16}O\text{-}C\text{-}{}^{16}O \rightarrow {}^{16}O\text{-}C\text{-}{}^{18}O + H_2^{16}O$$
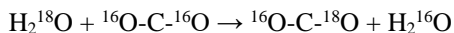
This isotope exchange reaction is known and has the effect of enriching the carbon dioxide with the oxygen isotope ^{18}O. The spontaneous exchange of the oxygen isotopes in the CO_2 and H_2O mixtures has been studied in aqueous solutions in a series of earlier

13

papers. In 1940, Mills and Urey[18] performed measurements for several pH values from acidic, through mildly alkaline media (leading to the prevalence of bicarbonate ions), up to very alkaline environments. They proved that the oxygen exchange in acidic and mildly alkaline solutions occurs through the formation of the carbonic acid by the simple hydration of CO_2. The mechanism of oxygen exchange between carbon dioxide and water following atmospheric sampling using glass flasks was explained in Refs.[24][28]. The oxygen isotope exchange between CO_2 and water adsorbed on Al_2O_3 or Fe_2O_3 was studied by Baltrusaitis et al.[27]. The rate constants of the spontaneous exchange in the solution are strongly temperature dependent. The mechanism of possible processes taking place on the surface of TiO2 is shown in Figure 6.
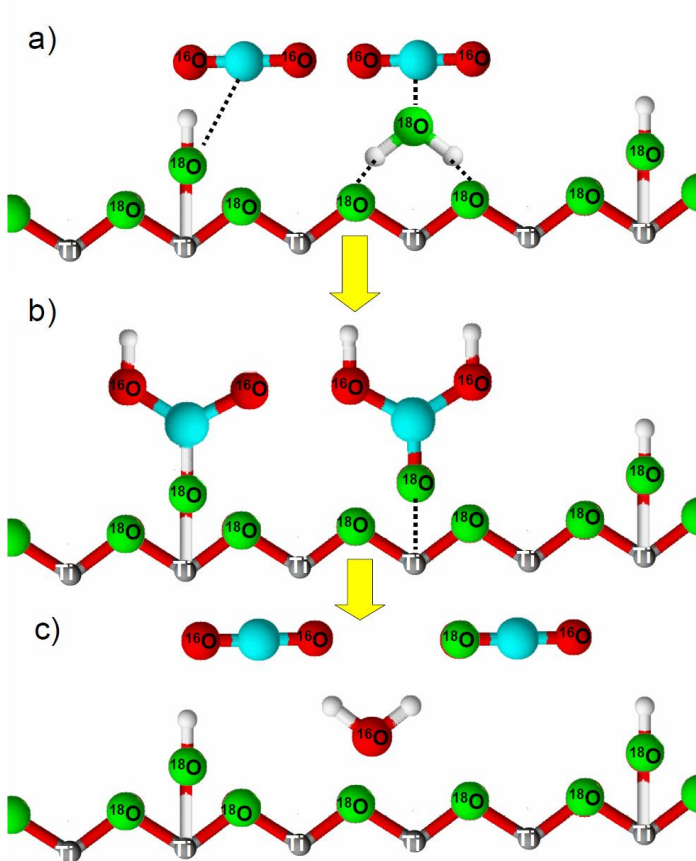
Fig. 6: Diagram of isotope exchange on the surface of crystalline $Ti^{18}O_2$. The surface layer is composed of Ti^{4+} onto which the ^{18}OH groups and $H_2^{18}O$ are bonded. The gaseous carbon dioxide reacts with water and OH groups, creating a hydrogen and dihydrogen complex bonded onto the Ti atoms. This complex breaks down after the laser irradiation or thermally at low pressure, back into molecules of $H_2^{16}O$, ^{16}O-C-^{16}O and partially also into ^{16}O-C-^{18}O.

1.4 The Spontaneous Oxygen Isotope Exchange on vacuum-annealed Ti^{18}O$_2$ (Sample T450)

The oxygen isotope exchange between C16O2 and Ti18O2 (sample T450) was examined by high resolution FTIR spectroscopy as in the case of the sample T200 discussed above. The isotopic exchange effects can be monitored either by observation of the envelope of the individual isotope absorption rotation-vibration bands or by observation of the individual rotation-vibration transitions of the ^{16}O-C-^{16}O, ^{18}O-C-^{16}O and ^{18}O-C-^{18}O molecules. Figure 8 (black curve) depicts a portion of the reference spectrum of the fundamental ν_3 band of carbon dioxide around 2300 cm^{-1}. (The other traces depict the spectra of the gas phase in a cell loaded with a Ti^{18}O$_2$ solid (0.8 g, sample T450). In this case, the T450 sample was calcined in-situ and transferred to the optical cell under vacuum (see Experimental Section). Subsequently, the cell was filled with 2 Torr of C^{16}O$_2$. Blue trace shows a spectrum of the gas phase measured immediately after the admission of C^{16}O$_2$. Green and red traces and show the spectra measured after 15 hours (green) and 50 hours (red), respectively.

From the spectrum measured immediately after mixing of both components (blue) it is clear that the oxygen exchange between the surface molecules of T450 Ti^{18}O$_2$ and oxygen in the C^{16}O$_2$ molecules is a very fast process. The obtained spectrum presents the rotation-vibration lines of ^{16}O-C-^{18}O together with the lines of ^{18}O-C-^{18}O.

16
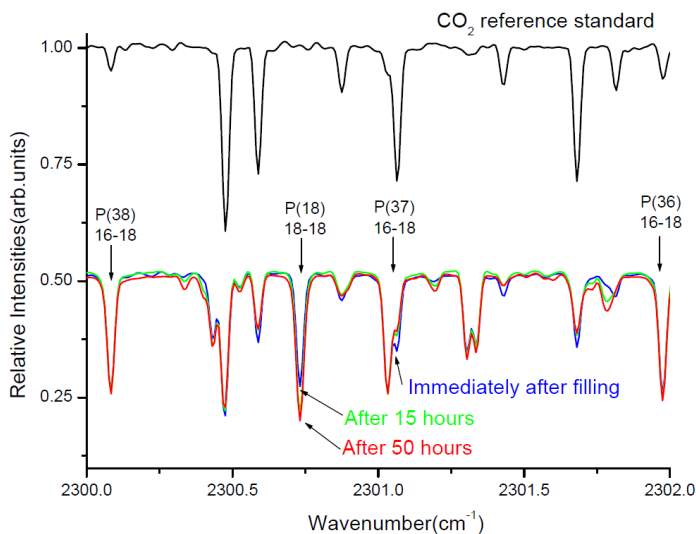
Fig. 7: Several rotation-vibration lines of the ν_3 band of $C^{16}O_2$ in the spectral range 2300-2302 cm^{-1} (reference spectrum - black) together with the spectra of carbon dioxide (2 Torr) measured immediately after the filling (blue), after 15 hours (green) and after 50 hours (red). The absorption cell contained 0.8g of $Ti^{18}O_2$ in the powder form, spread over the walls of the glass reaction cell.

The profiles of the individual lines of selected isotopologues (isolated lines in the spectrum) were fitted and quantified. The quantification of the spectra was carried out on the basis of calibration measurements of the absorption spectra of individual isotopologues (reference gases) of carbon dioxide at different pressures.
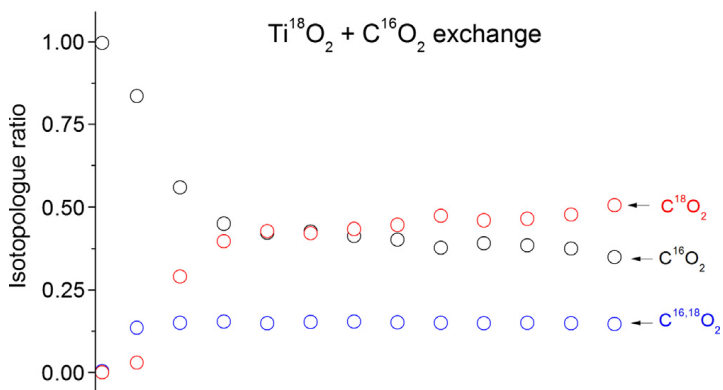
Fig. 8. The concentrations of individual isotopologues determined from the intensity profiles of the individual rotation-vibration lines are characterized by the exponential decrease of the ^{16}O-C-^{16}O isotopologue and the exponential increase of the ^{18}O-C-^{18}O isotopologue. The ^{18}O-C-^{16}O acts as an intermediate in the mixture and its concentration remains almost constant. The concentrations of the ^{18}O-C-^{16}O and ^{18}O-C-^{18}O isotopologues for time = 0 are given for their natural abundances.

2. Mechanism of Oxygen Exchange Between CO_2 and $TiO_2(101)$ Anatase

Conversion of CO_2 to marketable products using photocatalytic processes has received considerable attention in recent years, as part of the general portfolio of strategies considered to alleviate the environmental impact of greenhouse emissions.[29, 30].

A prerequisite for further scientific progress in this area is enhanced understanding of the interactions between CO_2 and TiO_2 surfaces. Among the methods used to obtain atomic scale insight into the evolution of the chemical intermediates on the oxide surface is oxygen isotope exchange. In the case of TiO_2 catalysts, this method has traditionally considered ^{18}O-isotope-labeled molecules interacting with regular $Ti^{16}O_2$ surfaces. This approach has been applied to investigate diffusion of vacancies in TiO_2,[30] evolution of O, CO, CO_2, and carbonate species on the TiO_2 surface[31] as well as the evolution of photocatalytic reactions on TiO_2-based materials.[15, 32, 33]

Recently the isotope exchange method has been extended to consider the reverse process in which ^{16}O-containing molecules interact with a solid oxide that is isotopically labeled. In this context, Civiš and collaborators[4] have demonstrated how isotopically pure $Ti^{18}O_2$ samples can be prepared from various Ti-precursors via hydrolysis using heavy-oxygen water, $H_2^{18}O$. Both anatase and rutile forms have been synthesized using either TiF_4 or $TiCl_4$ precursors, and formation of pure $Ti^{18}O_2$ isotopologues has been demonstrated based on analysis of Raman spectra.[34] Furthermore, the reactions of $C^{16}O_2$ with $Ti^{18}O_2$ anatase under both thermal- or photo-excitation conditions have been considered,[4, 35] and formation of methane and acetylene was observed in the presence of water upon UV irradiation. Following the chemical evolution of CO_2 on the oxide surface it has been demonstrated that $Ti^{18}O_2$ anatase samples annealed in vacuum at 450 °C can exchange oxygen with gaseous $C^{16}O_2$ leading to formation of $C^{18}O_2$ as the major product with a minor content of $C^{16}O^{18}O$.[4] Isotopic oxygen exchange has been suggested to take place by adsorption of gaseous $C^{16}O_2$ molecules at surface oxygen defects where they bind to a surface ^{18}O and form

bidentate CO_3 species with subsequent thermal release of either ^{16}O-C-^{18}O or ^{18}O-C-^{18}O species. (4) A similar CO_3 intermediate was assumed by Yanagisawa and Sumimoto(10) in their study of the oxygen exchange of $C^{18}O_2$ with vacuum-annealed $Ti^{16}O_2$ powders; however, specific details of the mechanism were not elaborated.

Formation of surface oxygen defects (V_O) on the anatase surface is a topic that has been reviewed several times over the past decade.(7)(36–38) It has been noted(36) that there is a smaller tendency for formation of V_O defects on the anatase (101) surface (the most stable surface of this polymorph) than on its counterpart, the (110) surface of rutile. This finding has been attributed to the lower stability of adjacent four-fold Ti^{3+} sites on the anatase (101) surface than of adjacent five-fold coordinated Ti^{3+} sites on the rutile (110) surface. Density functional theory (DFT)(37) calculations have demonstrated that the energy for forming an oxygen surface defect is about 0.5 eV greater than for forming a bulk vacancy. More recently, the distribution of surface oxygen defects created non-thermally by electron bombardment and monitored as function of temperature using a scanning tunneling microscope (STM) was reported.(38) In that study, it was found that surface defects start to migrate to subsurface sites at temperatures above 200 K. This study(38) also found that after an initial decrease in the density of surface defects, some surface defects reappeared either at the same sites or at different locations on the surface, indicating a back and forth movement of the oxygen defects among surface and subsurface sites. As noted by the authors of Ref(22), the results of the DFT calculations are hard to reconcile with the thermal equilibrium between subsurface and surface oxygen defects observed in STM experiments. However, it was noted that the calculations did not consider the effect of other subsurface defects upon the stability of the primary V_O defect, initially located on the surface.

The possibility to create surface oxygen defects and Ti^{3+} sites on anatase TiO_2 nanocrystals using mild conditions has been also reported. Specifically, work done in the Praserthdam group has shown that such surface defects can be created at mild temperatures either by changing the amount of oxygen fed during calcination(39) or by varying the water:alkoxide ratio during a sol-gel synthesis.(22) For samples synthesized using the latter method, the measured temperature programmed desorption (TPD) spectra of CO_2 indicate

the presence of broad peaks at 175 and 200 K. These peaks were assigned, respectively, to adsorption of CO_2 at regular Ti^{4+} and at Ti^{3+} vacancy sites.[40] This assignment was done in direct analogy with the 170 and 200 K TPD peaks recorded for CO_2 adsorbed on oxidized and reduced rutile(110).[41] Given the close correspondence between the TPD data on the anatase and rutile surfaces it can be expected that the binding energies of CO_2 on the anatase (101) surface closely resemble those on the rutile(110) surface. We note that zero-coverage adsorption energies of 11.59 and 12.90 kcal/mol have been determined for CO_2 on the fully oxidized and reduced rutile (110) surfaces, respectively.[41]

We have extend our previous theoretical investigation[41] of the adsorption of CO_2 on the oxidized and defective anatase (101) surface by including oxygen exchange between gaseous CO_2 and surface oxygen atoms. As shown in previous studies of adsorption of CO_2 on the rutile[20-23] and anatase[41] surfaces, an accurate description with almost quantitative agreement between experiments and theoretical predictions can be obtained if corrections for long-range dispersion interactions are included in the DFT calculations.

2.1 CO$_2$ Adsorption and Oxygen Exchange Reactions on the Defective (101) Anatase Surface for U=0 eV.

It was concluded in earlier experimental studies,[4, 9] that oxygen atom exchange between gaseous CO_2 and the anatase surface is mediated by formation of a carbonate species upon CO_2 adsorption at a surface V_O defect site. In order to test this hypothesis, we started from the analysis of the adsorption configurations of CO_2 at or near a Vo site on anatase(101) surface, in an attempt to identify promising candidate configurations for formation of the CO_3 species. In this subsection, we consider results obtained in the absence of the Hubbard U term correction; the effect of non-zero U corrections is considered in the following subsection.

A summary of the CO_2 binding configurations on the defective anatase(101) surface is presented in the left-hand side inset panels of Figure 9.
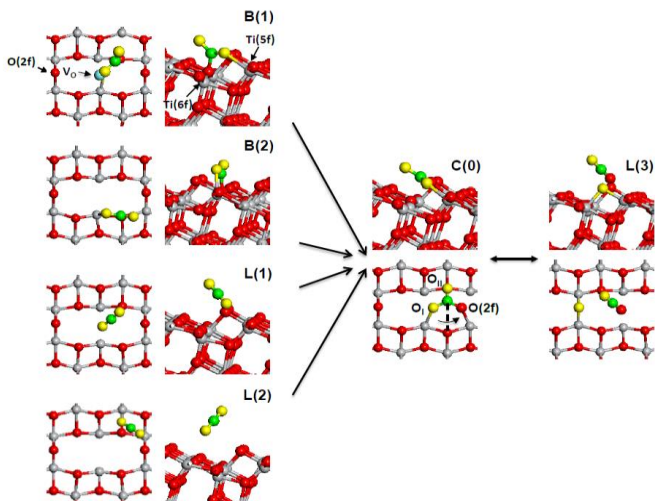
Figure 9. General scheme representing the initial, intermediate and final configurations involved in the oxygen exchange mechanism between CO_2 and a defective anatase (101) surface. The left panels illustrate side and top views of the adsorption configurations of CO_2 at a V_O site on the surface. The CO_2 molecule remains linear in L(**1**) and L(**2**) but is bent in B(**1**) and B(**2**) with formation of new bonds with Ti(5f) and O(2f) surface atoms. The intermediate panels indicate side and top views of the C(**0**) configuration. The right-side panels presents side and top views of a CO_2 molecule with an exchanged O atom adsorbed in a linear L(**3**) configuration which is symmetrically equivalent to L(**1**) with respect to C(**0**). For easy identification the O and C atoms of the original CO_2 molecule are depicted in yellow and green, respectively, while the O and Ti atoms of the surface are colored in red and gray, respectively. The location of the V_O site is indicated in light blue in the top left panel. For the C(**0**) configuration O_I denotes the O atom of CO_2 molecule closest to the surface which is bonded to a Ti(5f) atom while O_{II} indicates the nonbonded O atom of the CO_2 molecule.

As can be seen, near a surface V_O site, CO_2 can adsorb in either bent or linear configurations. In the former case (see

22

configurations B(**1**) and B(**2**)) covalent bonds between the adsorbed CO_2 molecule and surface atoms are formed, while in the latter case (see configurations L(**1**) and L(**2**)) the molecule is physisorbed on the surface.

The adsorption energies were calculated using the expression $E_{ads} = (nE_{CO_2} + E_{slab} - E_{(CO_2+slab)})/n$, where E_{CO_2} is the energy of the CO_2 molecule at its optimized gas-phase geometry, n represents the number of adsorbate molecules in the simulation cell, E_{slab} is the total energy of the slab, and $E_{(CO_2+slab)}$ is the total energy of the adsorbate/slab system. In this sign convention, positive adsorption energies correspond to stable configurations. The energy of the isolated CO_2 molecule was calculated using a cubic cell with sides of 12 Å.

In addition to the four configurations discussed above and which we reported previously in ref,(42) we present a new binding configuration C(**0**) with the CO_2 bound to the surface by 14.6 kcal/mol. This corresponds to a bent CO_2 molecule adsorbed at V_O site in a laying down configuration with formation of two new bonds, one with a surface Ti(5f) atom and a second with a nearby bridging O(2f) atom. The C(**0**) binding configuration corresponds to a CO_3-like species symmetrically bonded to two consecutive Ti(5f) atoms located in the top layer. As shown in the top view representation of C(**0**) in Figure 1, the resulting CO_3 entity has axial symmetry with respect to an axis passing through the C-OII bond of the original CO_2 molecule. Due to the axial symmetry, the O_I atom (represented in yellow in Figure 1) bonded to the Ti(5f) atom becomes practically symmetrical equivalent to the surface bridging O(2f) atom (represented in red). The O_{II} end of the molecule remains non-bonded to surface atoms as seen from the side view representation. Thus, this configuration appears to be an ideal candidate for promoting oxygen exchange.
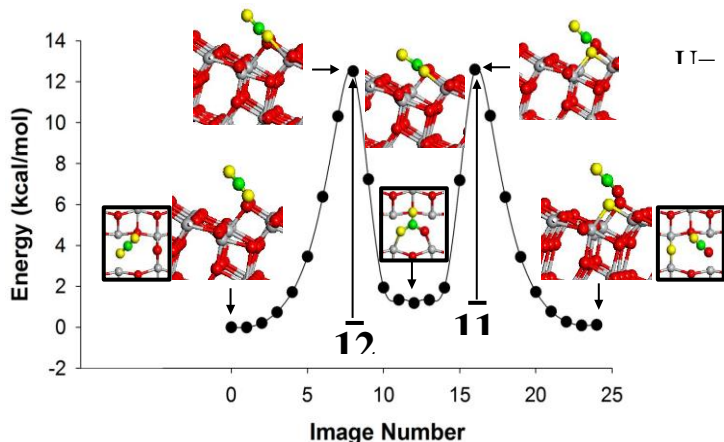
Figure 10. Minimum energy pathways for oxygen exchange between a CO_2 molecule and the anatase (101) surface via L(**1**)→C(**0**)→L(**3**) as determined from PBE-TS calculations with U=0 eV. Atomic configurations for specific images along the reaction pathway are indicated. The color legend of the atoms is the same as in Figure 9.

As shown in Figure 9 the energy profiles for L(**1**)→C(**0**) and L(**3**)→C(**0**) are essentially equivalent. The barriers for the entry L(**1**)→C(**0**) and for the exit C(**0**)→ L(**3**) steps are calculated to be 12.5 and 11.4 kcal/mol, respectively. These barriers can be easily overcome by thermal excitation under the experimental conditions.(34)

Overall, the results presented in this section based on PBE-TS DFT calculations give CO_2 binding energies which are consistent with the TPD experiments.(39) Additionally, the calculated barriers for the proposed sequence of steps L(**1**)→C(**0**)→L(**3**) have moderate values indicating that oxygen exchange could be initiated by thermal excitation at ambient conditions, in agreement with experimental measurements.(34)

As found in previous study, (34) the isotopic oxygen exchange reaction of $C^{16}O_2$ with reduced $Ti^{18}O_2$ anatase occurs at ambient temperature. As seen from the data in Figure 8, for U > 2.5 eV the calculations give large barriers (20.4-24.2 kcal/mol) for CO_2

elimination from the carbonate-like state. A barrier of this magnitude would make the exchange mechanism unlikely under thermal excitation at room temperature. Only in the case of U < 2.5 eV are the calculated barriers low enough to be consistent with oxygen exchange taking place at ambient temperature.

For U = 0 eV the calculated activation energies for the oxygen exchange mechanism between CO_2 and solid TiO_2 are small enough ($E_a < 12.5$ kcal/mol) to support initiation of the oxygen exchange at ambient temperature.

A final comment pertains to the oxygen exchange mechanism. As shown in this work a carbonate-like species C(**0**) can be formed at a surface V_O site, with the exchange taking place *via* a bridging O atom directly bonded to the CO_2 species. If the location of the vacancy on the crystal were to remain fixed during the experiments, only a limited number of CO_2 molecules could undergo oxygen exchange. However, experiments have shown that oxygen exchange between $C^{16}O_2$ molecules and solid $Ti^{18}O_2$ can convert a high fraction of the $C^{16}O_2$ molecules to $C^{18}O_2$. (34) This requires that there be a continuous supply of Vo sites on the oxide surface. As shown recently by Scheiber *et al.*,(38) following equilibration there is a continuous exchange of defects between surface and subsurface sites of anatase. Such a process would replenish ^{18}O atoms on the surface at defect sites, allowing for conversion of a large fraction of the $C^{16}O2$ molecules to $C^{18}O_2$.

2.2 Conclusion

The totally ^{18}O- isotope exchanged titanium dioxide, viz. $Ti^{18}O_2$ (anatase) was prepared from $TiCl_4$ and $H_2^{18}O$. The as received material, heat-treated at 200ºC still contained considerable amount of adsorbed HCl from the synthesis. This HCl was released into the environment composed of 2 Torr of CO_2. However, if the same material was calcined at 450ºC in high vacuum, the purified, HCl-free TiO^{18}_2 (anatase) was obtained. This vacuum annealed anatase exhibited spontaneous ^{18}O- isotope exchange the surrounding CO_2 which was monitored by high-resolution FTIR spectroscopy of the gas phase over the TiO^{18}_2 surface. Detailed investigation of the exchange reactions revealed:

After the irradiation of the T200 surface with the UV laser, additional rotation-vibration bands of methane, acetylene and water were identified in the gaseous phase.

The water molecules which are released or created in the gas phase reflect, that no exchange of oxygen atoms ^{18}O from the solid phase ($Ti^{18}O_2$) take place.

A small amount of $C^{16}O$ generated from the gaseous $C^{16}O_2$ by laser irradiation remains in the gas phase constant. The isotope exchange does not take place between the oxygen in the carbon monoxide molecule and the oxygen atom from the $Ti^{18}O_2$ structure.

The possible processes taking place on the surface of $Ti^{18}O_2$ can be summarized in the following way: ^{18}OH groups and $H_2^{18}O$ are bonded on the surface layer composed of Ti^{4+}. The gaseous carbon dioxide reacts with water and OH groups, creating a carbonate complex bonded onto the Ti atoms. This complex is breaking down after the laser irradiation or thermally at low pressure, back into molecules of $H_2^{16}O$, ^{16}O-C-^{16}O and partially also into ^{16}O-C-^{18}O.

Vacuum-annealed $Ti^{18}O_2$ (Sample T450) shows a very high spontaneous exchange activity with gaseous $C^{16}O_2$. Based on the spectral intensity and the isotopic exchange measurement, we are in good agreement with the proposal of the formation of the bidentate bonded carbonate as the major species for CO_3 on TiO_2. The surface layer vacuum-annealed $Ti^{18}O_2$ is composed of a nonstoichiometric mixture of Ti^{4+} and Ti^{3+} onto which the ^{18}O oxygen atoms are bonded. The calcination in vacuum creates vacancies. During the isotope exchange the ^{16}O oxygen from the gaseous ^{16}O-C-^{16}O bonds into the vacancy on the surface of the TiO_2 crystal and bidentate CO_3 from the CO_2 adsorption is formed. The ^{18}O oxygen from the surface layer is bonded to the carbon dioxide molecule and subsequently gaseous ^{16}O-C-^{18}O and ^{18}O-C-^{18}O are released.

3.   Methanogenesis

3.1 Photocatalytic Transformation of CO_2 to CH_4 on acidic surface of TiO_2 Anatase

Recently, many studies demonstrated that carbon dioxide can be converted to methane on TiO_2 surface by a photocatalytic process. We show that such a photo-reduction can be significantly affected by presence of an acidic proton in powdered samples of titania. Using in situ absorption gas-phase rovibrational spectroscopic detection of CH_4, CO and CO_2, we demonstrate the proton enhancement positively affects tranformation of intermediate derivates to methane during the photo-irradiation process via several reactions in which the electron transfer inside titania is coupled to oxygen transfer to the Ti^{3+} centers of TiO_2 structure. The yield of CH_4 or CO depends on the surface conditions on titania: the formation of CH_4 is boosted by a presence of adsorbed HCl, while the formation of CO is boosted by adsorbed solution of H_2SO_4.

3.2 Introduction

Due to the increasing greenhouse gases concentration in the atmosphere, global warming effect represents a substantial problem for our planet. Carbon dioxide, a product of excessive combustion of fossil fuels, belongs to the most significant atmospheric contributors. Beside other possible processes of CO_2 removal, a chemical conversion of carbon dioxide into energy containing fuel offers cheap and feasible solution. Such photocatalytic technologies towards carbon dioxide conversion into fuel have attracted an attention of many researchers and swiftly became promising in application. It is known that photo-irradiated metal oxides can reduce (with a small quantum yield) carbon dioxide with water adsorbed on the oxide surface to form highly energetic molecules such as methane, methanol, acetone, formaldehyde, formic acid, acetone and others depending on the specific conditions. (43),(44)
The photochemical reaction pathway from CO_2 to methane involves several reaction steps producing both stable and unstable molecular

27

intermediates.

The detailed description of the methanogenesis on titania (45), (46), (45) indicates the existence of charge-transfer reactions involving two or more electrons from the titanium dioxide(46),(47) or a different mechanism of one-electron reduction from the bulk solvent, which includes trapped electron Ti^{3+} centers on the titania surface.

Formation of surface oxygen defects (V_O) on the anatase surface is a topic that has been investigated several times over the past decade. (48), (19), (20), (49), (22), (50) It has been shown(19) that there is lesser tendency towards formation of V_O defects on the anatase (101) surface than on the (110) surface of rutile. This finding has been ascribed to the lower stability of adjacent 4-fold Ti^{3+} sites on the anatase (101) surface than of adjacent 5-fold-coordinated Ti^{3+} sites on the rutile (110) surface. Density functional theory (DFT) (49) calculations indicate that the forming of an oxygen surface defect needs about 0.5 eV higher energy than forming of a bulk vacancy.

To explain the importance of Ti^{3+} centers and their role in heteroatomic photocatalytic reactions on the surface of metal oxides, several studies have been carried out. Zapol et al. showed two fundamental reactions on Ti^{3+} centers: (45), (51)

$$Ti^{3+} + A_{ad} \rightarrow Ti^{4+} + A^{-\bullet} \qquad (1)$$
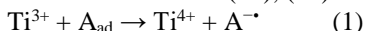
 Ti^{3+} surface centers occur with reactant and intermediate molecules serve as electron acceptors (A) that are adsorbed on these centers.

$$Ti^{3+} + RB_{ad} \rightarrow Ti^{4+}B^- + R^\bullet \qquad (2)$$
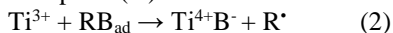
In addition to reaction (1) there is another class of electron-transfer reactions on oxide surfaces. These reactions occur only in certain types of molecular adsorbates, denoted as the RB adsorbates, where R is an organic group and B is a base that involves a heteroatom (such as O or N), for which the Ti^{3+} center becomes an acceptor, forming a bond to the heteroatom. The proposed reaction mechanism (2) has broad implications for various processes from photocatalytic energy conversion to methanogenesis and diagenesis in planetary chemistry on Mars or Saturn's moon Titan.

In our photochemical experiments, three UV broadband light sources (each of them 300 – 400 nm, λ(max) = 366 nm, 160 W, E27 Omnilux Lamp) in air flow cooled photo reactor vessel have been used to irradiate powdered TiO_2 in presence of 10 Torr of CO_2. Three types of samples have been prepared using TiO_2 materials as follows:

1) Pure crystalline TiO_2 anatase prepared in a closed all−glass vacuum apparatus from titanium tetrachloride (99.98% Aldrich) vapours hydrolysed with deionized water ice. The synthesis is described in details in our previous works.[16], [17], [52], [18], [53], [54] The sample is referred to as A100, indicating annealing temperature of 100°C after the synthesis. According to our previous results, such sample contains significant amount of HCl.

2) Pure crystalline TiO_2 anatase A100 additionally calcinated in a furnace at the temperature of 450 °C. This calcinated type is further referred as A450. According to our previous results, the calcination temperature of 450 °C removes all traces of HCl and water. This A450 titania sample has been mixed with 1 ml of 10 % H_2SO_4.

3) Comparative measurement has been performed with A450 without presence of acid. The irradiation and subsequent detection of products using FTIR spectrometry[55], [18], [56], [57], [58] have been conducted in situ in a 20 cm long (2.5 cm diameter) glass optical cell with CaF_2 windows equipped with a 25 cm long quartz tube finger where irradiation of the TiO_2 took place (see Figure 11). Samples were frozen at −5 °C and contacted with 10 Torr of CO_2. The quartz finger was placed into the irradiation vessel for 70 hours. The spectral measurements have been performed in selected time intervals using a Bruker IFS 125 HR spectrometer (CaF_2 beam splitter, InSb detector) in a spectral range from 2000 to 5000 cm^{-1}. 50 spectra have been accumulated with a resolution of 0.02 cm^{-1} using the Blackmann−Harris apodization function.
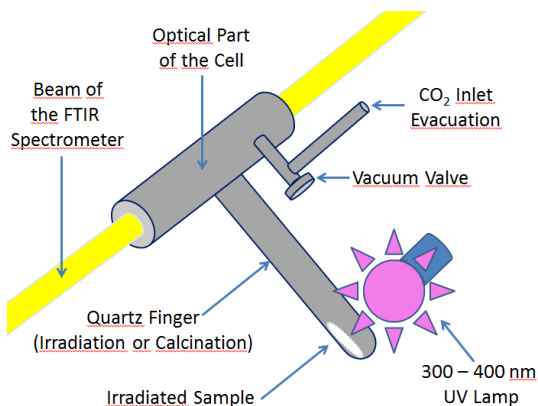
Figure 11. Scheme of the optical cell equipped with a quartz finger for calcination and irradiation.

Using FTIR spectra, methane and carbon monoxide have been identified as the main products in our irradiation experiments. Their formation was observed in both experiments with UV irradiation of CO_2 in presence of A100 (A100 contains   HCl from $TiCl_4$) and A450 sample (free of HCl) with 10 % H_2SO_4. Figure 12 shows the most significant spectral bands in our experiments. The upper three panels show methane, CO_2 and CO bands in our experimental samples, while the lower three panels show standard pure gas spectra of CH_4, CO_2 and CO measured on the same apparatus. Detail spectra of methane v_3 band measured after 37 and 70 hours of A100 irradiation are shown in the Figure 13. A comparative measurement was also performed with A450 in absence of any acid. In this case, methane concentration remained under detection limit. However, we detected 0.05 Torr of carbon monoxide.

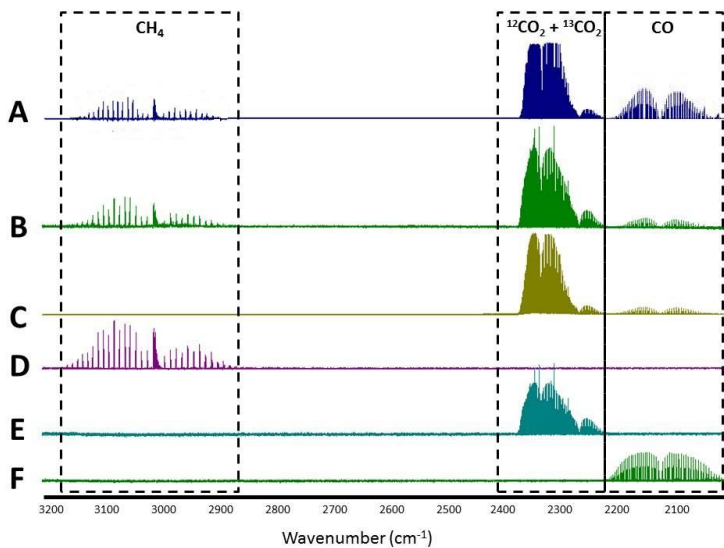Figure 12. Main absorption bands of CO_2 (v_3), methane (v_3) and CO after 70 hours of irradiation. Panel A shows an experiment with A450 + H_2SO_4, panel B A100, panel C and experiment with A450, panel D depicts standard spectrum of CH_4, panel E standard spectrum of CO_2 and panel F standard spectrum of CO. All spectra have been scaled to fit the picture, so abundances cannot be estimated form this picture.
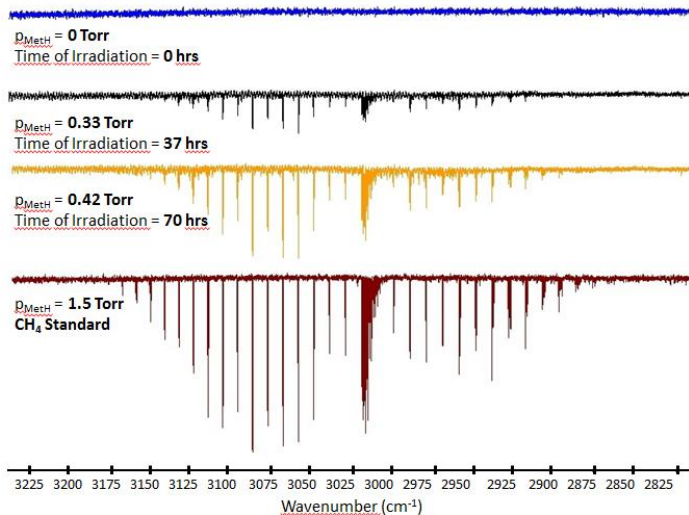
Figure 13. Time evolution of absorption ν_3 band of methane during irradiation of anatase A100 sample.

Time evolution of their gas phase concentrations is depicted in the Figure 14. At the end of the irradiation, the concentration of CH_4 in A100 anatase sample is significantly larger than that of CO. On the other hand, A450 sample with H_2SO_4 produces way more CO than CH_4 (the methane band is about 4 times weaker than that of CO and is therefore difficult to see in the picture Treatment of CO_2 in presence of A100 anatase (panel B) resulted in formation of 0.33 Torr of methane, while A450 (panel A) mixed with 10 % H_2SO_4 provided 0.26 Torr of CH_4. In case of A100 sample irradiation, the ratio of carbon monoxide to methane was about 80 times higher than in case of experiment with A450.

A — A100 with HCl

B — A450 with 10 % H₂SO₄

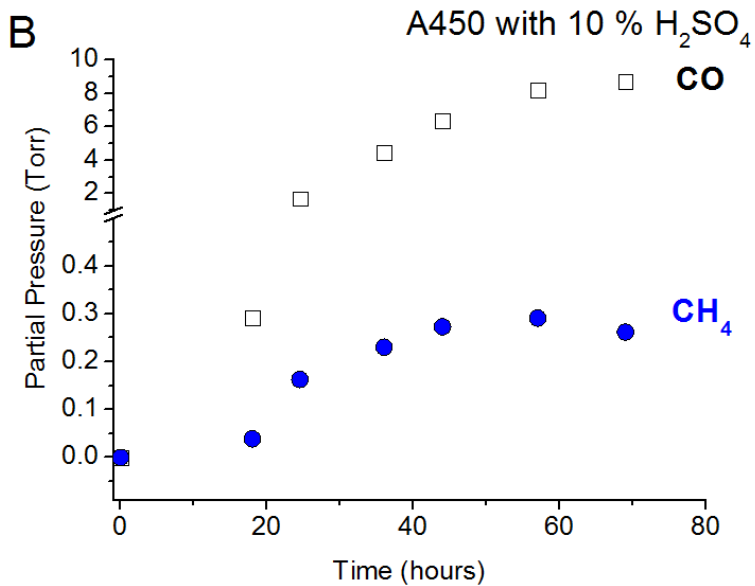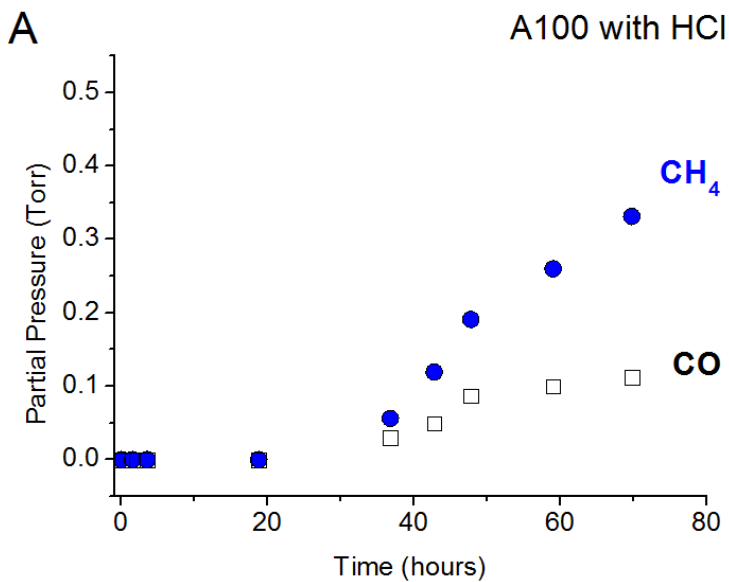Figure 14. Formation of main products in CO_2 treatment in presence of A100 with HCl is depicted in the panel A and in presence of A450 treated with 10 % H_2SO_4 in the panel B. Partial pressure (Torr) of CH_4 is marked in blue circles and CO is marked in black hollow squares.

Mechanism of CH_4 and CO formation has been discussed in details by Zapol et al.(45) A short scheme is shown in the Figure 15. CO_2 is adsorbed on the TiO_2 surface and accepts electron excited from the valence band to conduction band by UV radiation. Reaction with acidic proton leads to the formation of formyl HC-O radicals which subsequently transform to glyoxal OCH-HCO. In the following reaction steps, glyoxal again accepts protons and electrons and reacts with a donor of hydrogen (HCO, CH_3OH etc.)(59), (60), (61) forming acetaldehyde. During these reaction steps, water is released. In the final step which involves photolysis, acetaldehyde splits to CO molecule and methane. According to our results, this radical mechanism involving only CO_2 as a parent molecule in CO and CH_4 synthesis is very likely.
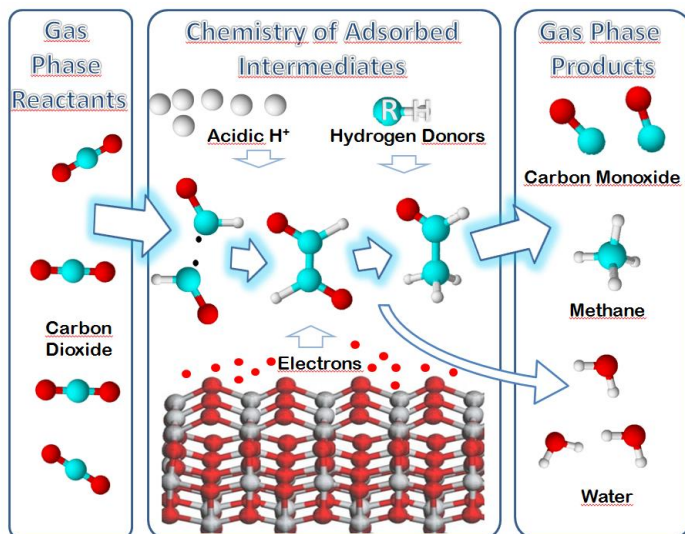

Figure 15. Scheme of CO_2 conversion to CO and CH_4 on the titania surface in the „Glyoxal Cycle" is shown in the panel A. Gas Phase

CO_2 molecules are adsorbed on the surface and all the products subsequently react with acidic protons, hydrogen donors and electrons coming from the conduction band. This chemistry is explained in details in Ref.(45)

In our previous studies and using ^{18}O isotopically labeled titania, we have demonstrated that oxygen in CO molecule is originating only from CO_2 and not from the TiO_2 lattice, which in other cases exhibits very unique oxygen mobility(17). However, the resulting ratio of the products depends also on a parent material and radiation intensity. Irradiation of A100, which contains HCl, resulted in CO: CH_4 ratio 1 : 3.5. Hence, this material is very efficient in CH_4 synthesis. Moreover, in our previous study, we also showed the synthesis of acetylene if XeCl laser is used as a source of radiation.(17) In contrary, a photo induced synthesis involving calcinated titania A450 in presence of 10 % H_2SO_4 led to CO:CH_4 ratio of 80:1. These results show that systems with oxygen excess (solutions of acids) are less favorable for methane synthesis than materials containing only directly adsorbed protons (from acid, an example of low temperature calcinated synthetic titania with HCl).

3.3 Conclusions

We demonstrated that CO_2 reduction to CH_4 is more efficient in presence of adsorbed hydrogen protons. In comparison to experiments with irradiation of titanina in presence of solution of acids, titania prepared by hydrolysis of $TiCl_4$ subsequently calcinated at low temperatures (100 ºC) seems to be more advantageous material due to significantly lower production rate of carbon monoxide. Although the industrial application of this technique is still very far off, it represents a possible solution for transformation of greenhouse gas CO_2 to CH_4 and CO containing fuel.

4. The origin of biomolecules on terrestrial planets from CO_2 cycle

The chemical evolution of early terrestrial planets is a long standing enigma which involves the uncertainty of chemical atmospheric

composition and plausibility of biomolecules synthesis. A new alternative pathway for the origin of methane Mars is suggested in this article. Through an interaction of soft ultraviolet radiation with a porous mineral surface, Martian and other planetary atmospheres rich in carbon dioxide can be abiotically converted into a mixture of methane and carbon monoxide through a process called 'methanogenesis'. A hypothesis was also tested that nucleobases and amino acids, can be formed in ~~subsequent~~ reprocessing of such ~~this~~ reduced atmosphere through impact-induced shock waves The proposed mechanism of methanogenesis may help answer the question of the the formation of methane and carbon monoxide by photochemical processes, the formation of biomolecules on early Earth and other terrestrial planets, and the source and seasonal variation of methane concentrations on Mars.

Historically, many arguments have been presented for both neutral (i.e. rich in CO_2, N_2, or H_2O,(62) supported by several modern geochemical findings)(63) and reducing (CH_4, NH_3, H_2, HCN, CO, etc.)(64) atmospheric compositions of the early Earth. Recent results comprehensively mapping terrestrial isotopic ratios of hydrogen and nitrogen show a difference from interplanetary gaseous or cometary material. They are rather in the range of values characterizing primitive meteorites. These findings suggest exogenous delivery of terrestrial water and atmosphere to the early Earth (broad review is supplied in(65)). It has been demonstrated that Earth lost its nebula-based protoatmosphere during the first 100 Myr - 500 Myr after its creation.(66) Nevertheless, a hydrogen envelope of a moderate mass around the early Earth may have acted during the first hundred Myrs as a shield against the deterioration of the atmosphere by the solar wind(66). A compromise scenarios incline towards a weakly reducing mixture consisting of volcanic gases such as CO_2, N_2, CO, and H_2O, with lesser amounts of H_2, SO_2, CH_4 and H_2S. However, as was mentioned above, the effects of exogenous delivery(67) of reducing compounds or Fischer-Tropsh processes(68) could have significantly contributed to even more reducing conditions (CO_2 + N_2 atmosphere with significant amounts of CH_4, NH_3, H_2S and H_2).(69, 70) Such a reducing state of the early terrestrial atmosphere is documented in ingenious zircons.(64) In accordance with several theories inclining to neutral gas composition of the early Earth's atmosphere, Mars can serve as a prototype of a The Martian

atmosphere represents a carbon dioxide rich environment which, might have been similar to the early Earth's. Recent in situ measurements of methane on Mars by the Curiosity rover reported significant variations in its concentration.(71) Across the Gale Crater, where the measurements were taken, methane was detected at a background concentration of ~0.7 ppb The abiotic synthesis of methane as a reducing gas in a natural carbon dioxide rich atmosphere is also highly relevant to studies of Earth's and Mars early stages of atmospheric evolution. Both planets contained water as a source of hydrogen, and they were exposed to a significant UV flux.(72) Even though its levels are debated, according to a comprehensive study by Chyba and Sagan,(73) energy dissipation from UV irradiation on the early Earth might have been two orders of magnitude more powerful (not effective) as an energy source than impact shock waves(59, 73–75) and four orders of magnitude more powerful than electric discharges.

Based on photochemical models and on the current understanding of the composition of the Martian atmosphere, methane exhibits a chemical lifetime 300−600 years, which is, on the geological scale a very short period.(76) This implies that there must be an active source of methane on Mars. Renyu Hu et al.(77) formulated three hypotheses for the origin of methane on Mars:

1. The first scenario is that the regolith in the Gale Crater adsorbs methane when dry and releases methane upon deliquescence during winter.

2. The second scenario is that microorganisms convert organic matter in the soil to methane. However, this scenario supposes the existence of extant life on Mars. Other explanations concerning life on Mars are summarized in (78).

3. The third scenario is that deep subsurface aquifers generate bursts of methane.

4. A fourth hypothesis has been formulated by Shkrob et al.(79) and is further developed in this article. The idea is that there could exist a complex UV-governed carbon chemistry:

5. Mars could be a planetary-sized "photoreactor", which decomposes carboxylated feedstock molecules producing

methane (Shkrob et al.(79)) while simultaneously, it could be a "photosynthetic" planet, where methane is generated from carbon dioxide over catalytic surfaces (Civiš, et al.,(80) Shkrob et al.(45)).

The methane synthesis from CO_2 is influenced by the amount of adsorbed water and adsorbed carbon dioxide on photocatalytic surfaces of mineral catalysts in combination with sufficient insolation. Mars is not currently shielded against UV radiation from the Sun. Such planet cannot serve as a direct prototype of the early Earth (as assumed by several authors in the case of Titan, the largest moon of Saturn)(81) but can be used as a model for the study of the pure photochemistry in planetary atmospheres in contact with large, mineral rich surfaces. This approximation can be used for further development of early Earth's atmospheric models.

The efficiency of the photocatalytic reduction of carbon dioxide was explored in this study on several mineral surfaces, of which two are most important: the widely used photocatalyst titania (anatase) and also the newly recognized photocatalyst montmorillonite, which exhibits a similar behaviour to titania according to this study. It should be noted that these minerals are present on Mars.(82) Montmorillonite or similar minerals are also present there.(83, 84) The presence of these constituents on early Earth is also likely in the discussed era.(85) An ability to synthesize reduced gases on the surface of this common material has been unknown so far. A study by Catling et al.(86) proposes a chlorine cycle on Mars. From this cycle, it is obvious that HCl is present on Mars. For this reason, HCl has been used in this study as a Mars-related acidic agent in reaction mixtures.

5. Origin of Methane on Mars

The photocatalytic reduction of CO_2 to methane may have strong implications for the origin of methane on Mars. It is important for this study to note that HCl has been detected on Mars.(87) Chlorination of the Martian surface has been estimated experimentally and perchlorates were first discovered in 2009 by Hecht et al. (88)

In this work, we present evidence for the photocatalytic UV-initiated reduction of CO_2 to CH_4 and CO under simulated Martian conditions

over anatase and montmorillonite. The main results are shown in figures 15 and 16.
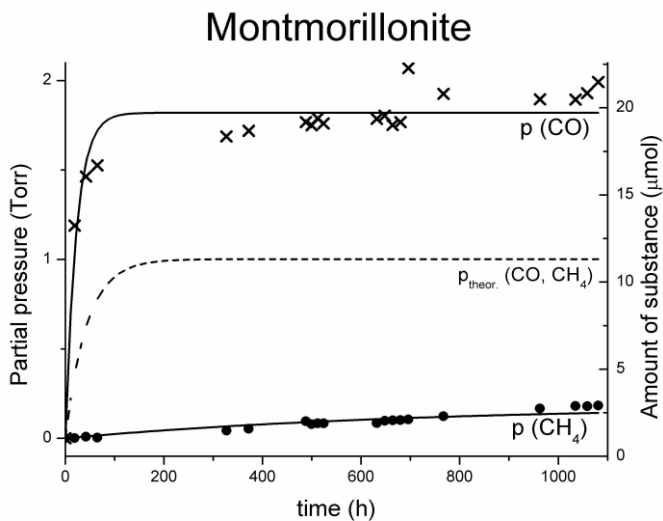
Montmorillonite

Figure 15: **Photocatalytic reduction over montmorillonite.** Gas phase analysis of sample containing montmorillonite as solid phase catalyst along with its pseudo first order kinetic fit. The figure also contains an expected theoretical concentration from an unperturbed reaction mechanism as discussed below.
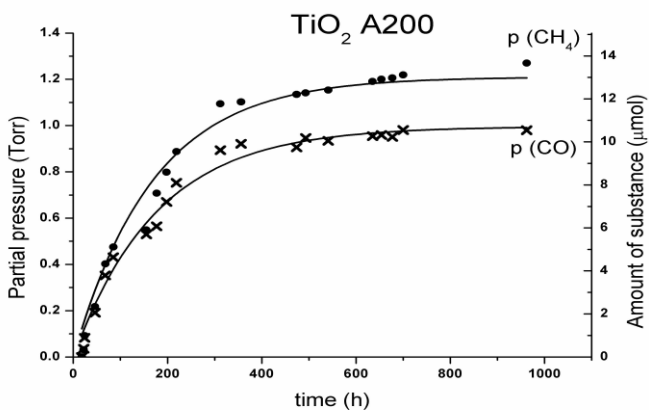
Figure 16: **Photocatalytic reduction over titania.** Gas phase analysis of sample containing TiO_2 anatase as solid phase catalyst along with its pseudo first order kinetic fit.

An important note to this topic is that the mineral regolith, which covers the surface of Mars, contains approximately 1% of titanium dioxide. Titanium dioxide is a well-known photocatalyst, and the high activity of this TiO_2 A200 sample in the presence of approximately 14 % (w/v) HCl has been demonstrated previously.(80) In contrast, such an effect over montmorillonite is unprecedented. The photocatalysis over titania was explained by three different mechanisms proposed in (89). They are called the glyoxal, formaldehyde and carbene pathways, of which the glyoxal pathway is in the best agreement with our data.

The UV flux on Mars, as modelled by Ronto et al.(90), is predicted to be currently lower than in the past. In fact, the current UV flux on Mars is approximately two or three orders of magnitude higher than that on Earth(90, 91) The details are shown in the chapter UV flux on Mars and Earth in the Supplementary Data. It may be assumed that such a combination of high UV irradiance through the thin Martian atmosphere and metal oxide photocatalysts turned the surface of this planet into a vast photoreactor.(92, 93)

In connection with Mars, as was discussed above, purely photochemical models (Lyman α radiation) predict resident times of methane of about 300 years.(94, 95) By taking into account the annual variation, however, it is clear that another process must play a major role in the methane decomposition. It has been estimated from observation of the concentration fluctuation that the lifetime of methane should be approximately 0.6 years.(96) The cause of this observed effect is probably the process of methanogenesis.

In fact, this hypothesis can be independently supported by plotting the seasonal atmospheric variations of CO_2, H_2O, and CH_4 on Mars.(97) The data, originally acquired by NASA's Mars Curiosity Rover and compiled to this plot by the authors, are shown in Fig. 17.
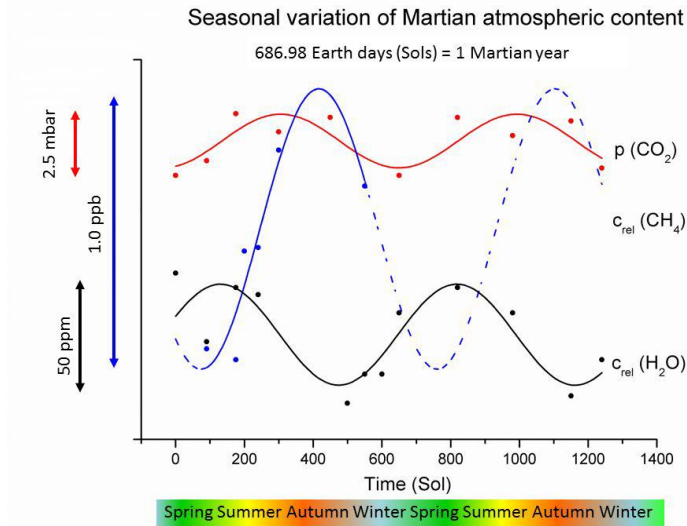
Figure 17: **Seasonal variation of atmospheric composition on Mars.** Seasonal variation of atmospheric composition on Mars. Seasonal variation of atmospheric pressure: CO_2 content (red), H_2O content (black) and CH_4 content (blue). Data points have been scaled to allow for visual comparison of their fits. The data were obtained by the NASA Mars Curiosity rover (2013–2014) and the OMEGA instrument on board the Mars Express. Sinusoidal curves in the plot are not fits, but represent only trends in the data. 686.98 Earth days (Sols) = 1 Martian year. C_{rel}, relative concentration.

For clarity, a sine function has been fitted to the data (period of 343.48005 sols, which represents half of the Martian year) to show the expected cycle of variation during one Martian year. Due to a lack of data, the fit has only an approximate purpose. Sol no. zero represents the beginning of the spring on the Martian northern hemisphere. The concentration of water vapour and the temperature rises steeply during spring. Water reaches its maximum concentration in the atmosphere at the end of spring. Methane concentration begins to rise at this point. At the beginning of

41

summer, the water content slowly decreases while the methane content in the atmosphere reaches its maximum. The methane content increase cannot be explained only by solar irradiation and a subsequent release because its maximum is observed at the end of autumn. More likely, the methane concentration is influenced by the amount of adsorbed water and adsorbed carbon dioxide on photocatalytic surfaces in combination with sufficient insolation. During the beginning of spring, insolation increases and adsorbed carbon dioxide and water are converted to methane. The process continues during summer. When insolation decreases at the end of summer, the effect is likely balanced by the adsorption of carbon dioxide and water as reactants. This is why the process continues during the beginning of autumn. At the end of autumn, the insolation becomes insufficient to induce photosynthesis of methane, and its concentration decreases.

The seasonal variation of CO on Mars should also be considered. This has been analysed by Encrenaz et al.(98) The authors analysed data from the Mars Express OMEGA instrument taken at various solar longitudes. Although the absolute values are disputed even by the authors, (up to 30% uncertainty), a trend in the data was discovered which shows that the CO mixing ratio in the atmosphere rises 1.5- to 2-fold (depending on the location of the measurement) during the northern summer.

To clarify the relevance of the reduction on Mars it may be said that it is possible to find all the primary constituents of the photocatalytic process: Regolith, which contains approximately 1% of TiO_2 anatase.(82, 83, 92), as well as smectite (clay mineral) or a mineral with similar atomic ratios and composition are abundant on Mars.(83) Photoactive clays are ubiquitous on Earth as well. Unfortunately, even though the presence of clays on Mars has been confirmed by the OMEGA instrument, which is a part of the Mars Express mission, its content in the overall geological composition of Mars has not yet been quantified. Detailed discussion may be found in the Supplementary Data Results from the Mars Curiosity rover.

Another key part to consider is the source of hydrogen/protons for the methane creation. When neutral environment is used, i.e. water is added to the mixture, the photocatalytic conversion has altered rates which strongly depend on the water content. From the empirical point of view, small amounts of water allow for the photocatalytic

reduction to take place. When the water content is larger, however, the active sites on the catalyst (only anatase and montmorillonite were so far tested) are probably occupied by the OH^- anions and the reduction is slowed down or negated completely. As was found earlier, however,[80] the photocatalytic reduction is significantly boosted by acidic environment. Addition of different acids to the mixture leads to different ratios between CO and CH_4. Here in this work, HCl was used, because it is naturally present on Mars.[86]

5.1 Early Earth – from reduced atmosphere to simple organics

UV light is considered to have been a very powerful source of energy in the primordial period of this planet.[99] Its energy dissipation[73] reached values orders of magnitude higher than lighting discharges or impact shock waves. However, its overall importance as a source of energy was estimated to have been lower than that of other energy sources for the possibly periodically alternating reducing and neutral conditions.[73]

Mineral catalysts such as montmorillonite or anatase are supposed to have been present on early Earth from the beginning of the chemical evolution of biomolecules and the emergence of life.[100] It can therefore be assumed that the early atmosphere of our planet was at least partly and locally photochemically transformed into CH_4. Recent results of the analysis of igneous zircons[64] of crustal origin show that the Hadean continental crust was more reduced than its modern counterpart and experienced progressive oxidation until 3.6 billion years ago,. The authors proposed that the conjunction of cold, wet and reduced granitic magmatism during the Hadean period produced CH_4 rich fluids, in addition to the CO and H_2 rich volcanic species produced by degassing. In fact, such "fluids" can also be accompanied by the photolytic production of CO and CH_4 over mineral surfaces. However, the exact calculation of the steady state balance between methane, carbon monoxide and carbon dioxide under conditions of early Earth is a challenging problem for planetologists.

To further extend the implications of the presence of a reduced atmosphere on the early Earth, the transformation of an atmosphere produced by the photocatalytic conversion of CO_2 to a mixture of

43

CO and CH$_4$ in the presence of acidic anatase, montmorillonite and water was explored. In our recent article,(59) a complete self-standing model on the formation of RNA−canonical nucleobases initiated by shock wave plasmas from an asteroid impact in a formamide rich environment was postulated. Impact shock waves are expected to be a large source of energy for chemical transformations under the conditions of early Earth.

During the early and late heavy bombardment era, our Earth was exposed to heavy bombardment by extraterrestrial matter with frequencies many orders of magnitude higher than today. On context of the origin of life on early Earth, it may be said that a common aspect of these high-energy (laser plasma, LIDB) induced reactions of the reduced atmospheres containing H, N, C and O is that it is typically possible to observe short-lived radicals - ·CN, ·NH, ·CH – and vibrationally excited CO. This means that, considering the estimated product yield from the laser shock wave and the bombardment frequency on early Earth, the formation of an HCN-rich atmosphere from the above mentioned mixture is possible. This approach is in agreement with the expectations proposed by Sagan and Chyba.(73) One pot synthesis of all nucleobases starting with the HCN atmosphere has never been demonstrated. Here, in the proposed mechanism, laser shock waves initiate further polymerization of HCN and the formation of all the canonical nucleobases and glycine. Such experiment was performed using a large hall laser PALS. Main results are shown in figure 18 and are discussed in detail in the methods. Detailed mechanisms, as well as exact GC-MS results are described in the Supplementary data Reaction mechanisms in the HCN-based synthesis and GC-MS Results sections.
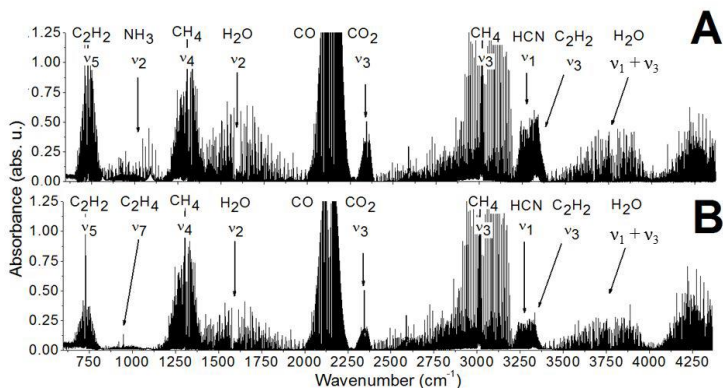
Figure 18: **High power laser irradiation.** Gas phase spectra of montmorillonite + HCl (Panel A) or TiO_2 A200 (Panel B), both in the presence of CO_2 + CO + CH_4 + N_2 treated by high-power laser PALS. Acetylene, ammonia, ethene and HCN were produced in the mixture due to the irradiation.

To relate these mechanisms to the chemistry of early Mars would be probably a bit far-fetched. The only observable relation may be based on the fact, the Earth and Mars are both terrestrial planets and that the atmosphere of early Mars was probably more like to Earth than it is today, i.e. Mars contained water in the past, and had a much denser atmosphere.

5.2 Conclusion

The laboratory experiments with the conversion of CO_2 to methane over titania and montmorillonite upon UV irradiation bring the evidence that the periodically alternating transformation of a CO_2 atmosphere to a reducing one containing CH_4 and CO and vice versa is possible on terrestrial type of planets with rich mineral surfaces exposed to large UV flux in presence of acidic water. This conversion must be considered in models of initial early atmosphere transformations of the early Mars and Earth as well as in explaining the seasonal atmospheric variation on current Mars. Importantly, it is not possible to ultimately proclaim that the Earth´s early atmosphere was globally reducing.

A neutral atmosphere containing CO_2 can be locally converted over photocatalytic surfaces of anatase, montmorillonite (or possibly other minerals) into a mixture of reduced gases, in particular CO and CH_4, by soft UV radiation with a wavelength maximum at 350 nm. The process is significantly boosted by an acidic surface. Current conditions on Mars are in favour of this process. This photoreduction may therefore explain the seasonal variation and the origin of methane on Mars. Furthermore, by comparison with the current conditions and planetary chemistry of the CO_2 rich atmosphere on Mars (and possibly the Saturn's moon Titan), it seems probable that this same process may have occurred on the early Earth and occurs on many bodies throughout the whole of the universe. Thus created reduced atmosphere can be again transformed under different conditions back to CO_2.

Furthermore, a pathway is here shown for the formation of RNA nucleobases from the reduced (CH_4 and CO enriched) gas mixture in the presence of parent photoactive minerals (montmorillonite, anatase, etc.) in shock wave plasma. The pathway involves hydrogen cyanide, acetylene, cyanoacetylene and ammonia which were all detected in the experiment by high resolution infrared spectroscopy. In the proposed chemical transformation, ·CN, ·NH and vibrationally excited CO molecule together with water play the dominant role. The RNA nucleobases, along with urea and glycine were detected by GC-MS. The shock wave plasma chemistry is relevant to the early Earth conditions due to a high frequency of asteroid impacts during the Late Heavy Bombardment period.

To sum up, a complete scenario is here proposed (for detailed information please refer to the Supplementary data section and refs. (75)(101)(102) for the transformation of a CO_2 rich atmosphere into reactive reducing mixture of CH_4 and CO and a subsequent synthesis of RNA nucleobases, glycine and urea from this very mixture. This pathway is relevant to both early Earth and Mars.

6. References

1.   Aresta Editor M ed. (2010) *Carbon Dioxide as Chemical Feedstock* (Wiley-VCH Verlag GmbH & Co. KGaA, Weinheim).

2.   Usubharatana P, McMartin D, Veawab A, Tontiwachwuthikul P (2006) Photocatalytic process for CO2 emission reduction from industrial flue gas streams. *Ind Eng Chem Res* 45(8):2558–2568.

3.   Thompson TL, Diwald O, Yates JT (2004) Molecular oxygen-mediated vacancy diffusion on TiO2(110) - new studies of the proposed mechanism. *Chem Phys Lett* 393(1–3):28–30.

4.   Liao LF, Lien CF, Shieh DL, Chen MT, Lin JL (2002) FTIR study of adsorption and photoassisted oxygen isotopic exchange of carbon monoxide, carbon dioxide, carbonate, and formate on TiO2. *J Phys Chem B* 106(43):11240–11245.

5.   Wu T, Kaden WE, Anderson SL (2008) Water on rutile TiO2(110) and Au/TiO2(110): Effects on an mobility and the isotope exchange reaction. *J Phys Chem C* 112(24):9006–9015.

6.   Henderson MA (1996) Structural sensitivity in the dissociation of water on TiO2 single-crystal surfaces. *LANGMUIR* 12(21):5093–5098.

7.   YANAGISAWA Y (1995) Oxygen-exchange between CO2 and metal (Zn and Ti) oxide powders. *ENERGY Convers Manag* 36(6–9):443–446.

8.   Yanagisawa Y, Ota Y (1991) Thermal and photo-stimulated desorption of chemisorbed oxygen molecules from titanium-dioxide surfaces. *Surf Sci* 254(1–3):L433–L436.

9.   SATO S (1987) Hydrogen and oxygen isotope exchange-reactions over illuminated and nonilluminated TiO2. *J Phys Chem* 91(11):2895–2897.

10.   Yanagisawa Y, Sumimoto T (1994) Oxygen-exchange between CO2 adsorbate and TiO2 surfaces. *Appl Phys Lett* 64(24):3343–3344.

11.   Henderson MA, Epling WS, Peden CHF, Perkins CL (2003) Insights into photoexcited electron scavenging processes on TiO2 obtained from studies of the reaction of O-2 with OH groups adsorbed at electronic defects on TiO2(110). *J Phys Chem B* 107(2):534–545.

12. Muggli DS, Falconer JL (1999) UV-enhanced exchange of O-2 with H2O adsorbed on TiO2. *J Catal* 181(1):155–159.

13. Felipe Montoya J, Peral J, Salvador P (2011) Surface Chemistry and Interfacial Charge-Transfer Mechanisms in Photoinduced Oxygen Exchange at O-2-TiO2 Interfaces. *CHEMPHYSCHEM* 12(5):901–907.

14. Mikhaylov R V, Lisachenko AA, Titov V V (2012) Investigation of Photostimulated Oxygen Isotope Exchange on TiO2 Degussa P25 Surface upon UV-Vis Irradiation. *J Phys Chem C* 116(44):23332–23341.

15. Pichat P, Courbon H, Enriquez R, Tan TTY, Amal R (2007) Light-induced isotopic exchange between O-2 and semiconductor oxides, a characterization method that deserves not to be overlooked. *Res Chem Intermed* 33(3–5):239–250.

16. Kavan L, et al. (2011) Oxygen-isotope labeled titania: (TiO2)-O-18. *Phys Chem Chem Phys* 13(24):11583–11586.

17. Civiš S, Ferus M, Kubát P, Zukalová M, Kavan L (2011) Oxygen-Isotope Exchange between CO2 and Solid (TiO2)-O-18. *J Phys Chem C* 115(22):11156–11162.

18. Civiš S, et al. (2012) Photochemistry and gas-phase FTIR spectroscopy of formic acid interaction with anatase (TiO2)-O-18 nanoparticles. *J Phys Chem C* 116(20):11200–11205.

19. Hebenstreit W, Ruzycki N, Herman GS, Gao Y, Diebold U (2000) Scanning tunneling microscopy investigation of the TiO2 anatase (101) surface. *Phys Rev B* 62(24):R16334–R16336.

20. He Y, Dulub O, Cheng H, Selloni A, Diebold U (2009) Evidence for the Predominance of Subsurface Defects on Reduced Anatase TiO2(101). *Phys Rev Lett* 102(10). doi:10.1103/PhysRevLett.102.106105.

21. Cheng HZ, Selloni A Energetics and diffusion of intrinsic surface and subsurface defects on anatase TiO2(101). *J Chem Phys* 131(5):54701–54703.

22. Scheiber P, et al. (2012) (Sub)Surface Mobility of Oxygen Vacancies at the TiO2 Anatase (101) Surface. *Phys Rev Lett* 109(13):136103.

23. Suriye K, Jongsomjit B, Satayaprasert C, Praserthdam P (2008) Surface defect (Ti3+) controlling in the first step on

the anatase TiO2 nanocrystal by using sol-gel technique. *Appl Surf Sci* 255(5):2759–2766.

24. Suriye K, Praserthdam P, Jongsomjit B (2007) Control of Ti3+ surface defect on TiO2 nanocrystal using various calcination atmospheres as the first step for surface defect creation and its application in photocatalysis. *Appl Surf Sci* 253(8):3849–3855.

25. Thompson TL, Diwald O, Yates JT (2003) CO2 as a probe for monitoring the surface defects on TiO2(110) - temperature-programmed desorption. *J Phys Chem B* 107(42):11700–11704.

26. Sorescu DC, Al-Saidi WA, Jordan KD (2011) CO2 adsorption on TiO2(101) anatase: A dispersion-corrected density functional theory study. *J Chem Phys* 135(12). doi:10.1063/1.3638181.

27. Sorescu DC, Lee J, Al-Saidi WA, Jordan KD (2011) CO2 adsorption on TiO2(110) rutile: Insight from dispersion-corrected density functional theory calculations and scanning tunneling microscopy experiments. *J Chem Phys* 134(10). doi:104707 10.1063/1.3561300.

28. Lee J, Sorescu DC, Deng X (2011) Electron-Induced Dissociation of CO2 on TiO2(110). *J Am Chem Soc* 133(26):10066–10069.

29. Chen X, Mao SS (2007) Titanium dioxide nanomaterials: Synthesis, properties, modifications, and applications. *Chem Rev* 107(7):2891–2959.

30. Kavan L (2006) Nanocrystalline TiO2 for Solar Cells and Lithium Batteries. *Disclosing Materials at the Nanoscale*, Advances in Science and Technology. (Trans Tech Publications), pp 20–29.

31. Winter ERS (1968) Exchange Reactions of Oxides. *J Chem Soc A* (12):2889–2902.

32. Novakova J (1970) Isotopic exchange of oxygen O-18 between gaseous phase and oxide catalysts. *Catal Rev* 4(1):77-.

33. Nakamura R, Nakato Y (2004) Primary intermediates of oxygen photoevolution reaction on TiO2 (rutile) particles, revealed by in situ FTIR absorption and photoluminescence measurements. *J Am Chem Soc* 126(4):1290–1298.

34. Bogdanoff P, Alonso-Vante N (1994) A kinetic approach of competitive photoelectrooxidation of HCOOH and H2O on TiO2 anatase thin-layers via online mass detection. *J Electroanal Chem* 379(1–2):415–421.

35. Zhang M, et al. (2009) Oxygen Atom Transfer in the Photocatalytic Oxidation of Alcohols by TiO2: Oxygen Isotope Studies. *Angew CHEMIE-INTERNATIONAL Ed* 48(33):6081–6084.

36. Kalamaras CM, Panagiotopoulou P, Kondarides DI, Efstathiou AM (2009) Kinetic and mechanistic studies of the water-gas shift reaction on Pt/TiO2 catalyst. *J Catal* 264(2):117–129.

37. Henderson MA (1995) Formic-acid decomposition on the (110)-microfaceted surface of TiO2(100) - Insights derived from 18O-labeling studies. *J Phys Chem* 99(41):15253–15261.

38. Jimenez C, Perriere J, Palacio C, Enard JP, Albella JM (1993) Transformation of titanium nitride in oxygen plasma. *Thin Solid Films* 228(1–2):247–251.

39. Brenninkmeijer CAM, et al. (2003) Isotope effects in the chemistry of atmospheric trace compounds. *Chem Rev* 103(12):5125–5161.

40. Hadjiivanov K, Lamotte J, Lavalley JC (1997) FTIR study of low-temperature CO adsorption on pure and ammonia-precovered TiO2 (anatase). *LANGMUIR* 13(13):3374–3381.

41. Mills GA, Urey HC (1940) The Kinetics of Isotopic Exchange between Carbon Dioxide, Bicarbonate Ion, Carbonate Ion and Water1. *J Am Chem Soc* 62(5):1019–1026.

42. Rothman LS, et al. (2009) The HITRAN 2008 molecular spectroscopic database. *J Quant Spectrosc Radiat Transf* 110(9–10, SI):533–572.

43. Inoue T, A F, Konishi S, Honda K (1979) Photoelectrocatalytic Reduction of Carbon Dioxide in Aqueous Suspensions of Semiconductor Powders. *Nature* 277(5698):637–638.

44. Demont A, Abanades S (2015) Solar thermochemical conversion of CO2 into fuel via two-step redox cycling of non-stoichiometric Mn-containing perovskite oxides. *J*

Mater Chem A 3(7):3536–3546.

45. Shkrob IA, Marin TW, He H, Zapol P (2012) Photoredox Reactions and the Catalytic Cycle for Carbon Dioxide Fixation and Methanogenesis on Metal Oxides. *J Phys Chem C* 116(17):9450–9460.

46. Dimitrijevic NM, et al. (2011) Role of Water and Carbonates in Photocatalytic Transformation of CO2 to CH4 on Titania. *J Am Chem Soc* 133(11):3964–3971.

47. Dimitrijevic NM, Shkrob IA, Gosztola DJ, Rajh T (2012) Dynamics of Interfacial Charge Transfer to Formic Acid, Formaldehyde, and Methanol on the Surface of TiO2 Nanoparticles and Its Role in Methane Production. *J Phys Chem C* 116(1):878–885.

48. Sorescu DC, Civis S, Jordan KD (2014) Mechanism of oxygen exchange between CO2 and TiO2(101) anatase. *J Phys Chem C* 118(3):1628–1639.

49. Cheng H, Selloni A (2009) Energetics and diffusion of intrinsic surface and subsurface defects on anatase TiO(2)(101). *J Chem Phys* 131(5). doi:10.1063/1.3194301.

50. Setvin M, et al. (2013) Reaction of O-2 with Subsurface Oxygen Vacancies on TiO2 Anatase (101). *Science (80-)* 341(6149):988–991.

51. Shkrob IA, Dimitrijevic NM, Marin TW, He H, Zapol P (2012) Heteroatom-transfer coupled photoreduction and carbon dioxide fixation on metal oxides. *J Phys Chem C* 116(17):9461–9471.

52. Civiš S, et al. (2015) Oxygen atom exchange between gaseous CO2 and TiO2 nanoclusters. *J Phys Chem C* 119(7):3605–3612.

53. Ferus M, et al. (2014) Spontaneous and photoinduced conversion of CO2 on TiO2 anatase (001)/(101) surfaces. *J Phys Chem C* 118(46):26845–26850.

54. Civiš S, et al. (2014) Room temperature spontaneous conversion of OCS to CO2 on the anatase TiO2 surface. *Chem Commun* 50(57):7712–7715.

55. Civiš S, Ferus M, Zukalova M, Kavan L, Zelinger Z (2013) The application of high-resolution IR spectroscopy and isotope labeling for detailed investigation of TiO2/gas interface reactions. *Opt Mater (Amst)* 36(1, SI):159–162.

56. Ferus M, Cihelka J, Civis S (2008) Formaldehyde in the environment - Determination of formaldehyde by laser and photoacoustic detection. *Chem List* 102(6):417–426.

57. Civis S, et al. (1998) Submillimeter-wave spectral lines of negative ions (SH- and SD-) identified by their Doppler shift. *J Chem Phys* 108(20):8369–8373.

58. Boháček P, et al. (1990) Composition of phases and phase mixtures of the Bi-Sr-Ca-Cu-O system. *Phys C* 171(1–2):108–120.

59. Ferus M, et al. (2014) High-energy chemistry of formamide: A unified mechanism of nucleobase formation. *Proc Natl Acad Sci* . doi:10.1073/pnas.1412072111.

60. Ferus M, et al. (2011) HNC/HCN Ratio in Acetonitrile, Formamide, and BrCN Discharge. *J Phys Chem A* 115(10):1885–1899.

61. Ferus M, Matulkova I, Juha L, Civis S (2009) Investigation of laser-plasma chemistry in CO-N-2-H2O mixtures using O-18 labeled water. *Chem Phys Lett* 472(1–3):14–18.

62. Kasting JF (1993) Earth's Early Atmosphere. *Science (80-)* 259(5097):920–926.

63. Delano JW (2001) Redox history of the Earth's interior since approximately 3900 Ma: implications for prebiotic molecules. *Orig Life Evol Biosph* 4–5(31):311–341.

64. Yang X, Gaillard F, Scaillet B (2014) A relatively reduced Hadean continental crust and implications for the early atmosphere and crustal rheology. *Earth Planet Sci Lett* 393. doi:10.1016/j.epsl.2014.02.056.

65. Marty B (2012) The origins and concentrations of water, carbon, nitrogen and noble gases on Earth. *EARTH Planet Sci Lett* 313:56–66.

66. Lammer H, et al. (2014) Origin and loss of nebula-captured hydrogen envelopes from `sub'- to `super-Earths' in the habitable zone of Sun-like stars. *Mon Not R Astron Soc* 439(4):3225–3238.

67. de Niem D, Kuehrt E, Morbidelli A, Motschmann U (2012) Atmospheric erosion and replenishment induced by impacts upon the Earth and Mars during a heavy bombardment. *Icarus* 221(2):495–507.

68. Sekine Y, et al. (2006) An experimental study on Fischer-

Tropsch catalysis: Implications for impact phenomena and nebular chemistry. *Meteorit Planet Sci* 41(5):715–729.

69.   Hashimoto GL, Abe Y, Sugita S (2007) The chemical composition of the early terrestrial atmosphere: Formation of a reducing atmosphere from CI-like material. *J Geophys Res* 112(E5):E05010.

70.   Schaefer L, Jr. BF (2007) Outgassing of ordinary chondritic material and some of its implications for the chemistry of asteroids, planets, and satellites. *Icarus* 186(2):462–483.

71.   Webster CR, et al. (2015) Mars methane detection and variability at Gale crater. *Science (80-)* 347(6220):415–417.

72.   Sullivan WT, Baross J (2007) *Palents and life: The Emerging science of astrobiology* (Cambridge University Press; 1 edition).

73.   Chyba C, Sagan C (1992) Endogenous Production, Exogenous Delivery and Impact-Shock Synthesis of Organic Molecules - an Inventory for the Origin of Life. *Nature* 355(6356):125–132.

74.   Koeberl C (2006) Impact processes on the early Earth. *Elements* 2(4):211–216.

75.   Ferus M, et al. (2014) High-Energy Chemistry of Formamide: A simpler way for nucleobase formation. *J Phys Chem A* 118:719–736.

76.   Nair H, Allen M, Anbar AD, Yung YL, Clancy RT (1994) A Photochemical model of the Martian Atmosphere. *Icarus* 111(1):124–150.

77.   Hu R, Bloom AA, Gao P, Miller CE, Yung YL (2016) Hypotheses for Near-Surface Exchange of Methane on Mars. *Astrobiology* 16(7):539–550.

78.   Levin G V, Straat PA (2016) The Case for Extant Life on Mars and Its Possible Detection by the Viking Labeled Release Experiment. *Astrobiology* 16(10):798–810.

79.   Shkrob IA, Chemerisov SD, Marin TW (2010) Photocatalytic Decomposition of Carboxylated Molecules on Light-Exposed Martian Regolith and Its Relation to Methane Production on Mars. *Astrobiology* 10(4):425–436.

80.   Civiš S, et al. (2016) Photocatalytic transformation of CO2 to CH4 and CO on acidic surface of TiO2 anatase. *Opt Mater (Amst)* 56(SI):80–83.

81. Raulin F, McKay C, Lunine J, Owen T (2009) Titan's Astrobiology. *Titan from Cassini-Huygens*, ed Brown, RH and Lebreton, JP and Waite J (Springer, PO BOX 17, 3300 AA DORDRECHT, NETHERLANDS), pp 215–233.

82. Bell JF (2008) *The Martian Surface-Composition, Mineralogy, and Physical Properties* doi:10.1017/CBO9780511536076.

83. Clark III BC, et al. (2007) Evidence for montmorillonite or its compositional equivalent in Columbia Hills, Mars. *J Geophys Res - Planets* 112(E6). doi:10.1029/2006JE002756.

84. Ehlmann BL, Edwards CS (2014) Mineralogy of the Martian Surface. *Annual Review of Earth and Planetary Sciences*, Annual Review of Earth and Planetary Sciences., ed Jeanloz R (ANNUAL REVIEWS), pp 291–315.

85. Hazen RM, et al. (2008) Mineral evolution. *Am Mineral* 93(11–12):1693–1720.

86. Catling DC, et al. (2010) Atmospheric origins of perchlorate on Mars and in the Atacama. *J Geophys Res - Planets* 115. doi:10.1029/2009JE003425.

87. Gordon PR, Sephton MA (2016) Organic Matter Detection on Mars by Pyrolysis-FTIR: An Analysis of Sensitivity and Mineral Matrix Effects. *Astrobiology* 16(11):831–845.

88. Hecht MH, et al. (2009) Detection of Perchlorate and the Soluble Chemistry of Martian Soil at the Phoenix Lander Site. *Science (80-)* 325(5936):64–67.

89. Habisreutinger SN, Schmidt-Mende L, Stolarczyk JK (2013) Photocatalytic Reduction of CO2 on TiO2 and Other Semiconductors. *Angew Chemie-Internation Ed* 52(29):7372–7408.

90. Ronto G, et al. (2003) Solar UV irradiation conditions on the surface of Mars. *Photochem Photobiol* 77(1):34–40.

91. Schuerger AC, Mancinelli RL, Kern RG, Rothschild LJ, McKay CP (2003) Survival of endospores of Bacillus subtilis on spacecraft surfaces under simulated martian environments: implications for the forward contamination of Mars. *Icarus* 165(2):253–276.

92. Chun SFS, Pang KD, Cutts JA, Ajello JM (1978) Photocatalytic Oxidation of Organic Compounds on Mars. *Nature* 274(5674):875–876.

93. Quinn RC, Zent AP (1999) Peroxide-modified titanium dioxide: A chemical analog of putative Martian soil oxidants. *Orig Life Evol Biosph* 29(1):59–72.

94. Wong AS, Atreya SK, Encrenaz T (2003) Chemical markers of possible hot spots on Mars. *J Geophys Res* 108(E4). doi:10.1029/2002JE002003.

95. Krasnopolsky VA, Maillard JP, Owen TC (2004) Detection of methane in the martian atmosphere: Evidence for life? *Icarus* 172(2):537–547.

96. Mumma MJ, et al. (2009) Strong Release of Methane on Mars in Northern Summer 2003. *Science (80-)* 323(5917):1041–1045.

97. Webster G, Brown D, Cantillo L (2016) Second Cycle of Martian Seasons Completing for Curiosity Rover. Available at: http://mars.nasa.gov/msl/news/whatsnew/index.cfm?FuseAction=ShowNews&NewsID=1908 [Accessed January 3, 2017].

98. Encrenaz T, et al. (2006) Seasonal variations of the martian CO over Hellas as observed by OMEGA/Mars Express. *Astron Astrophys* 459(1):265–270.

99. Cockell CS (1998) Biological effects of high ultraviolet radiation on early Earth - a theoretical evaluation. *J Theor Biol* 193(4):717–729.

100. Ferris JP, Hill ARJ, Liu R, Orgel LE (1996) Synthesis of long prebiotic oligomers on mineral surfaces. *Nature* 381(6577):59–61.

101. Civiš S, et al. (2016) TiO2-catalyzed synthesis of sugars from formaldehyde in extraterrestrial impacts on the early Earth. *Sci Rep* 6:23199.

102. Šponer JE, et al. (2016) Prebiotic synthesis of nucleic acids and their building blocks at the atomic level - merging models and mechanisms from advanced computations and experiments. *Phys Chem Chem Phys* 18(30):20047–20066.

7. Citační profil autora

Citační souhrn pro publikace, které jsou součástí předkládané práce

(dle Web of Science, ke dni 6.12.2017)

Celkový počet publikací   14

Celkový počet citací   273

Celkový počet citací bez autocitací (včetně spoluautorů)

         108

Citační souhrn

(dle Web of Science, ke dni 6.12.2017)

Celkový počet publikací   163

Celkový počet citací   1528

Celkový počet citací bez autocitací (včetně spoluautorů)

         961

h-index   22

researcher ID: F-5189-2014